XIST Regulates Breast Cancer Stem Cells by Activating Proinflammatory IL-6 Signaling

Yuxi Ma
University of Michigan–Ann Arbor
Yongyou Zhu
University of Michigan–Ann Arbor
Li Shang
University of Michigan–Ann Arbor
Yan Qiu
University of Michigan–Ann Arbor
Na Shen
University of Michigan–Ann Arbor
Qingxuan Song
University of Michigan–Ann Arbor
Jun Li
University of Michigan–Ann Arbor
Max S. Wicha
University of Michigan–Ann Arbor
Ming Luo (mingluo@med.umich.edu)
University of Michigan–Ann Arbor

Research Article

Keywords: XIST, let-7, Interleukin-6 (IL-6), STAT3 activation, Epithelial and Mesenchymal CSCs

Posted Date: August 24th, 2022

DOI: https://doi.org/10.21203/rs.3.rs-1975545/v1

Abstract

Background

Aberrant expression of XIST, a long noncoding RNA initiating X chromosome inactivation (XCI) during early embryogenesis, is a common feature of breast cancer (BC). However, the roles of post-XCI XIST in breast carcinogenesis remain elusive.

Methods

In this study, we examined the expression of XIST in human BC cell (BCC) lines across the spectrum of BC subtypes. We then investigated the effect of knockdown (KD) of aberrantly expressed XIST in luminal and triple-negative (TN) BCCs on tumor growth, cancer stem cell (CSC) activities, and global gene expression. We identified the most significantly altered genes and pathways in $ALDH^-$ bulk tumor cells and $ALDH^+$ CSCs upon XIST KD and validated the roles of these genes in regulating $ALDH^+$ epithelial (E) versus $CD24^{-/lo}CD44^{+/hi}$ mesenchymal (M) CSCs. Lastly, we conducted miRNA array and luciferase reporter assays to define the molecular mechanisms of XIST in CSC regulation.

Results

Doxycycline (DOX) induced XIST KD markedly inhibits spheroid/colony forming capacity, tumor growth and tumor-initiating potential. This phenotype is attributed to impaired E-CSC in luminal and E- and M-CSC activities in TN BCCs. Gene expression profiling demonstrates that XIST KD most significantly affects cytokine-cytokine receptor interactions, resulting in markedly suppressed expression of proinflammatory cytokines IL-6 and IL-8 in the bulk of tumor cells. Exogenous IL-6, but not IL-8, rescues the reduced sphere-forming capacity and proportion of $ALDH^+$ CSCs in luminal and TN BCCs following XIST KD. This suggests a mechanism whereby XIST regulates IL-6 production by bulk tumor cells, which then acts in a paracrine manner on $ALDH^+$ CSCs that display elevated IL-6 receptor (IL6R) expression. XIST functions as a molecular sponge for MicroRNA let-7a-2-3p to derepress IL-6 expression, which in turn promotes self-renewal of $ALDH^+$ CSCs by inducing STAT3 activation and expression of key CSC factors including c-MYC, KLF4 and SOX9.

Conclusions

This study supports a novel role of XIST by derepressing let-7 controlled paracrine IL-6 proinflammatory signaling to promote CSC self-renewal.

Introduction

Cancer-stem like cells (CSCs), also called tumor initiating cells (TICs), promote tumorigenesis, disease progression, therapeutic resistance, and metastasis[1, 2]. In breast cancer (BC) and other malignancies, elevated aldehyde dehydrogenase ($ALDH^+$) activity is widely used to identify a highly tumorigenic cell population with capacities of self-renewal and multilineage differentiation, driving primary tumor growth and distant metastases [3–8]. Distinct from more quiescent basal/mesenchymal CSCs characterized by $CD24^{-/lo}CD44^{+/hi}$ marker expression [9], CSCs characterized by high ALDH activity display an epithelial-like (E), proliferative phenotype [10]. These $ALDH^+$ CSCs, designed as E-CSCs, express high level of phosphorylated STAT3 with nuclear localization [11], suggesting a critical role of STAT3 signaling in maintaining this proliferative CSC population.

Tumor cells and their microenvironment co-evolve to drive tumor growth and progression[12]. Paracrine signaling between distinct subsets of tumor cells and between tumor cells and stromal cells constantly modulates tumorigenic CSCs [13, 14]. Proinflammatory cytokines, such as IL-1, IL-6, and IL-8, play critical roles in the induction and maintenance of CSCs by activating STAT3/NFκB signaling pathways[15–19]. For instance, transient activation of the Src oncoprotein induces a high level of IL-6 production in immortalized breast epithelial cells, which in turn promotes tumorigenesis and generation of CSCs[17]. Moreover, IL-6 is able to convert differentiated bulk tumor cells into CSC-like cells in multiple molecular subtypes of BC[16], providing support for a causal role of IL-6 in tumorigenesis and cancer progression by inducing and/or maintaining cancer stemness.

The human *X-inactive specific transcript*, or *XIST*, encodes a 17 kb long noncoding RNA (lncRNA), which coats one of the two X chromosomes in female mammals to initiate gene silencing, thereby preventing gene dosage imbalance between females and males[20, 21]. In addition to its well-established role in X chromosome inactivation (XCI) during early embryogenesis, accumulating evidence suggests that aberrant XIST expression in post-XCI somatic cells plays a role in tumor development and progression. For example, genetic deletion of *XIST* in mouse hematopoietic and human mammary epithelial cells promotes the formation of highly aggressive myeloproliferative neoplasm and $HRAS^{G12V}$-driven mammary carcinoma respectively [22, 23], suggesting a role of *XIST* expression from the inactive X chromosome (Xi) in protecting somatic cells from oncogenesis. However, in late stage breast tumors or established BC cell lines, the Xi, or Barr body, is commonly absent, presumably due to the loss of Xi and replication of the active X chromosome (Xa) [24] and/or epigenetic erosion of the Xi [25], leading to the formation of XIST clouds in the nucleus deficient in XCI [26]. Supporting this abnormal function of XIST in post-XCI tumor cells, XIST expression in a wide variety of cancer cells suppresses or promotes tumor growth and/or metastasis [27–29]. Such divergent roles of XIST in cancer development and progression may reflect the fact that XIST functions as a major molecular sponge to repress a plethora of oncogenic or tumor suppressive MicroRNAs (miRNAs) and lncRNAs, leading to suppression or promotion of tumor growth and metastatic progression in a highly context-dependent manner [27–29].

In parallel with the findings that XIST is aberrantly expressed in BC cells [24, 25], high XIST expression in BC confers treatment resistance and poor patient outcomes. For instance, low expression of XIST correlates with cisplatin hypersensitivity and predicts long recurrence-free survival of HER2-negative,

stage III BC patients treated with intensive platinum-based chemotherapy [30]. In patients with BRCA1-deficient BC, high XIST expression predicts poor outcomes after high-dose alkylating chemotherapy[31]. This association of high XIST expression and chemoresistance suggests a role of aberrant XIST expression in promoting CSCs, which display intrinsic resistance to a variety of therapeutic agents. Indeed, in a study to evaluate histone deacetylase inhibitors (HDACi) as potential anti-CSC therapy, only the BC cells with low XIST expression exhibit HDACi response in mouse xenograft models, and this response is associated with a significant reduction of CSCs [32]. Despite this evidence, an understanding of how elevated XIST expression promotes CSCs remains elusive.

In this study, we examined XIST expression across a spectrum of BC cell lines representing different BC subtypes and investigated the impact of DOX-inducible KD of XIST on the maintenance of $ALDH^+$ E- and $CD24^{lo}CD44^{hi}$ M-like CSCs, as well as tumor growth and tumor-initiating potential in mouse xenograft models of luminal and TNBC. We demonstrate that XIST acts as a master regulator of cytokine-cytokine receptor interactions and drives IL-6 expression from $ALDH^-$ bulk tumor cells to regulate $ALDH^+$ CSCs in a paracrine fashion. XIST directly binds and suppresses let-7a-2-3p, a member of the let-7 family of miRNAs with tumor suppressor functions [33, 34], leading to markedly elevated IL-6 expression in $ALDH^-$ BCCs and, to a lesser extent, in $ALDH^+$ CSCs. IL-6 derived from the bulk $ALDH^-$ BCCs preferentially binds to IL6R on $ALDH^+$ CSCs to induce STAT3 activation and expression of key stemness factors c-MYC, KLF4 and SOX9, promoting self-renewal of $ALDH^+$ CSCs.

Materials And Methods

Cell Culture

SUM159 and SUM149 BC cells were cultured in Ham's F-12 (ThermoFisher Scientific) supplemented with 5% FBS (ThermoFisher Scientific), 5 µg/mL insulin (Sigma-Aldrich, St. Louis, MO), 1µg/mL hydrocortisone (Sigma-Aldrich), and 1x antibiotic-antimycotic (ThermoFisher Scientific, 100x). MCF7 cells were grown in EMEM medium (ATCC) supplemented with 10% FBS, 1x antibiotic-antimycotic, and 10 µg/mL insulin (Sigma-Aldrich). BT20, MDA-MB-231, MDA-MB-468, MDA-MB-157 and SKBR3 were cultured in DMEM-high glucose (Gibco) supplemented with 10% FBS and 1x antibiotic-antimycotic. Vari068, HCC38, HCC70, HCC1937, HCC1954, T47D and BT474 were maintained in RPMI1640 medium (ThermoFisher Scientific) supplemented with 10% FBS and 1x antibiotic-antimycotic. All the BC cell lines are cultured at 37°C under 5% CO_2 in a humidified chamber and are mycoplasma-free.

ALDEFLUOR Assay, Cell Labeling and Flow Cytometry

The ALDEFLUOR™ (STEMCELL Technologies Inc, Vancouver, Canada) kit was used to detect aldehyde dehydrogenase (ALDH) enzymatic activity following manufacturer's instructions. Briefly, single cells suspended at $1x10^6$ cells/mL in Aldefluor buffer are incubated with 5uL of BODIPY-aminoacetaldehyde (BAAA) for 40 minutes at 37°C, and 5uL of diethylaminobenzaldehyde (DEAB) was added along with BAAA as negative control. Aldefluor-labeled cells were resuspended in Aldefluor buffer containing 1µg/mL

of 4', 6-diamidino-2-phenylindole (DAPI, Sigma) to discriminate live from dead cells. To detect M-CSC-like cells in DOX-treated MCF7, HCC70 and SUM159 BCCs expressing shXIST hairpin or SCR sequence, antibodies against human CD24 (BV421-conjugated, 1:50, BD Biosciences) and CD44 (APC-conjugated, 1:200, BD Biosciences) were used to label the cells in cold room for 30 minutes and then washed with 1xHBSS buffer supplemented with 2% FBS. A MoFlo Astrios Cell Sorter (Beckman Coulter) equipped with six lasers (354nm, 405nm, 488nm, 561nm, 594nm, and 640nm) and twenty-five fluorescent detectors was used for FACS analysis and sorting at the Flow Cytometry Core Facility of the University of Michigan.

RNA Extraction and Quantitative Real-Time PCR (qRT-PCR) Assays

Total RNA and miRNA were extracted using RNeasy and miRNeasy Mini kit (Qiagen) respectively. Stem-loop qRT-PCR analysis for miRNA expression was performed with Taqman miRNA assay using probe ID listed in Table S1. RNU24 was used as endogenous control to normalize miRNA expression. Thermal cycling conditions for Taqman miRNA assay include an enzyme activation step (95°C for 10 min) and 40 cycles of amplification at 95°C for 15s followed by 60°C for 1min.

For mRNA/lncRNA expression, cDNA synthesis was performed on total RNA (10ng-1µg) using the High-Capacity cDNA Reverse Transcription Kit (ThermoFisher Scientific). cDNA samples were analyzed using TaqMan Universal Master Mix (for TaqMan probes) or Power SYBR® Green PCR Master Mix (for SYBR green primers) on an ABI PRISM 7900HT Real-Time PCR system (Applied Biosystems) according to manufacturer's instructions. Commercial sources and sequences of primers used for qRT-PCR of mRNA/lncRNA expression are listed in Table S1. Gene expression of lncRNA/mRNAs was normalized to GAPDH.

shRNAs and Lentiviral Infection

DOX-inducible lentiviral shRNA clones against human XIST (GE Dharmacon, V2THS_92229, V3SH11258_245457769, V3SH11258_245651017, V3SH11258_ 245601352) or a scrambled sequence (SCR) were packaged at the University of Michigan Vector Core. SUM159, HCC70 and MCF7 BC cells were infected with lentiviruses in the presence of polybrene (8µg/mL, Millipore) and the medium containing lentiviruses was replaced with fresh medium after 20 hours of lentiviral infection. Puromycin (Invitrogen) selection was performed at a final concentration of 1.0 µg/mL (for MCF7) or 2.5µg/mL (for HCC70 and SUM159) for 2 weeks to establish DOX-inducible shXIST or SCR cell lines.

MTT Assay

SCR and shXIST expressing cells were seeded at a density of 2,000 cells per well in 96-well plates for overnight and cultured with or without DOX (1 µg/mL, Sigma-Aldrich) for 2, 4, or 6 days. After DOX treatment, MTT solution was added to each well and incubated for 3 hours. After removing supernatant, cells in each well were solubilized by adding 150 µL of DMSO. OD absorbance of each condition at 590 nm was measured with a plate reader, and cell growth rate was plotted.

3D Soft Agar Assay

5% agarose gel (0.25g Ultrapure agarose in 5ml 1xHBSS) was melted in a microwave and cooled to 42 ˚C in water bath. 5 mL of 5% agarose gel was then mixed with 20ml of prewarmed cell culture medium to make 1% agarose gel. The 1% agarose gel was diluted with cell culture medium at 1:1 ratio to make a 0.5% base gel, which was poured into 6-well plates at 2 mL per well. The 1% agarose gel was diluted with cell culture medium at 1:2 ratio to make a 0.33% agarose top gel, and $2x10^4$ pTripz-shXIST-MCF7 cells or $7.5x10^3$ pTripz-shXIST-SUM159 cells were mixed with 2 mL of top gel and poured on the top of the base gel per well into 6-well plates. Cells embedded in 0.33% agarose gel were incubated at 37˚C for 2–4 weeks and fed with 2 mL of completed medium per well containing with or without 1µg/mL of DOX twice a week. Plates were stained with 0.005% Crystal Violet for 1 hour, and then washed with dH_2O. Colonies were imaged with a dissection microscope and counted with ImageJ.

Tumorsphere Formation Assay

SUM159 (10 cells/well) or MCF-7 (20 cells/well) BCCs expressing shXIST or SCR sequence were sorted into 96-well ultra-low attachment plate (Corning) containing 120 µL/well of completed human MammoCult medium (StemCell Technologies) supplemented with doxycycline (Sigma-Aldrich), 4 µg/mL heparin (StemCell Technologies), 1µg/mL hydrocortisone (Sigma-Aldrich) and 1x antibiotic-antimycotic (Thermo Fisher Scientific) and cultured at 37°C under 5% CO_2 for 14 days. For tumorsphere rescue assays, SUM159/MCF7-shXIST or SCR cells cultured in completed MammoCult medium containing DOX (1µg/mL) for 3 days in 96-well ultra-low attachment plates were supplemented with 50 ng/mL of exogenous IL-6 or IL8 (BioLegend) and continued to cultivate for 11 days. Tumorspheres with diameter ≥ 40µm were counted and photographed using an optical microscope with a 10x optical lens.

Western Immunoblotting

Total protein from cells or spheroids was extracted with 1xRIPA buffer (Cell Signaling Technology) supplemented with protease and phosphatase inhibitor cocktail (ThermoFisher Scientific). Cell lysates (20ug per lane) were leaded and subjected to SDS-PAGE with Bolt™ 4–12% Bis-Tris Plus Gel, blotted onto PVDF Membrane (ThermoFisher Scientific), and then blocked with 2% BSA in TBST buffer for 1 hour before incubation with primary antibodies (all from Cell Signaling Technology) against STAT3 (9139S), pSTAT3 (9145S), NFκB p65 (8242S), pNFκB p65 (3033S), c-MYC (18583S), SOX2 (3579S), SOX9 (82630S), OCT4 (2750S) and KLF4 (12173S). β-actin expression was probed with monoclonal antibody against β-actin (Sigma) as loading control. Membrane was rinsed three times in TBST for 5 minutes each time and incubated with HRP-conjugated rabbit or mouse secondary antibodies (Cell Signaling Technology). Protein bands were visualized using WesternBright Sirius Chemiluminescent Detection Kit (Advansta).

Next-Generation RNA Sequencing and Gene Expression Profiling

$ALDH^-$ and $ALDH^+$ cells isolated from DOX-untreated SUM159-shXIST BCCs were treated with or without DOX for 3 days, and total RNA from each cell sample was extracted and subjected to next generation

RNA sequencing (RNAseq) at the University of Michigan DNA Sequencing Core. RNA abundance and integrity were determined by a Nanodrop-ND-1000 spectrophotometer (ThermoFisher Scientific) and an Agilent 2100 Bioanalyzer (Agilent Technologies), respectively. Only samples of total RNA with an RNA integrity number (RIN) > 9 were used for RNAseq. Sequencing read quality was assessed utilizing FastQC. Reads were aligned against the human reference genome (GRCh37) to generate spliced alignments. We conducted differential expression testing on the assigned read counts per gene utilizing edgeR. To reduce the dispersion of the dataset due to lowly expressed genes, genes with a mean aligned read count less than five across all samples were excluded from analysis. Normalized counts per million were estimated utilizing the “cpm” function in edgeR, and differences in expression of genes were estimated using the generalized linear modeling function glmLRT. Genes were considered differentially expressed between cell populations at a false discovery rate (FDR) with adjusted p-value < 0.05. Differences in gene expression and signaling pathways were visualized by volcano plotting and pathway interaction mapping was developed by iPathwayGuide (https://advaitabio.com/ipathwayguide/).

MicroRNA Array Analysis

$ALDH^-$ and $ALDH^+$ cells isolated from DOX-untreated SUM159-shXIST cells were treated with or without (CTL) DOX at 1μg/ml for 3 days, miRNAs from each sample were extracted using miRNeasy Mini kit (Qiagen) and analyzed by GeneChip™ miRNA 4.0 Array (ThermoFisher Scientific) according to manufacturer’s instructions. miRNA-containing total RNA (300 ng) was biotin-labeled using the FlashTag Biotin RNA Labeling kit (Afymetrix, USA) and hybridized in the GeneChip Hybridization Oven 640 (Affymetrix, USA) at 48°C for overnight. After washed and stained in the GeneChip Fluidics Station 450 (Afymetrix, USA), arrays of different samples were scanned with a GeneChip Scanner 3000 7G (Afymetrix, USA) and signal strength was evaluated using the Expression Console Software (EC) v1.2 (ThermoFisher Scientific). To identify differentially expressed miRNAs in $ALDH^-$ and $ALDH^+$ cells treated with or without DOX, acquired array data were analyzed using Multi Experiment Viewer (MeV v4.9.0; The Institute for Genomic Research) and miRNAs with an absolute value of fold change ≥ 0.5 were identified as potential miRNAs significantly changed upon DOX-induced XIST KD.

miRNA Mimic/Inhibitor/DNA Transfection and Luciferase Reporter Assay

hsa-let-7a-2-3p mimic (ID: MC11174) vs. control (Cat#: 4464058), and miRNA inhibitors against human let-7a-2-3p (ID: AM11174), miR-374b-5p (ID: AM11339), miR-181c-5p (ID: AM10181), and miR1303 (ID: AM13799) vs. negative control (Cat#: AM17010) were obtained from ThermoFisher Scientific. Wild-type XIST cDNA fragments containing let-7a-2-3p binding sites 1 or 2 were generated by PCR from SUM159 BCC cDNAs, which is generated with the High-Capacity cDNA Reverse Transcription Kit (Life Technologies) and were inserted into the PmirGLO Dual-Luciferase miRNA Target Expression Vector (Promega, E1330). The mutagenesis of seed region in Site 2 was completed by overlap extension PCR. Overlap extension primer are (the underlined is mutant site of seed region): Overlap forward (F1) 5’-GAATAAAACTTTCTGTCGCAGCAGTATTGTCTCTACAAAATTC-3’; Overlap reverse (R1) 5’-GAATTTTGTAGAGACAATACTGCTGCGACAGAAAGTTTTATTC-3’. Sequences of the cDNA fragments

containing WT site 1 and 2 as well as mutated site 2 are shown in Table S2. For luciferase reporter assay, SUM159 cells were seeded into 96-well plates overnight and then transfected with the luciferase reporter plasmid plus *let-7a-2* mimic or control using Lipofectamine 3000 (ThermoFisher Scientific). 48 hours post transfection, luciferase activity was measured with the Dual-Luciferase Reporter Assay Kit (Promega, E2920). Firefly luciferase activity was normalized to Renilla to rule out the differences in transfection efficiency. Data were shown as fold change over control samples.

Tumor Growth in Mammary Xenograft Model of NOD/SCID Mice

NOD/SCID mice were bred in-house and housed in pathogen-free rodent facilities at the University of Michigan. All supplies (cages, chow, and sterile water) were autoclaved, and all experiments were conducted according to standard protocol approved by the University Committee on the Use and Care of Animals. 5 x10^5 MCF7 and 5 x10^4 SUM159 cells were injected into the 4th mammary fat pads of 6-week-old female NOD/SCID mice with 6–10 mice included in each cohort. For mice transplanted with MCF7 cells, 17β-estradiol pellet (Cat# SE-121, 60-day release, 0.18 mg/pellet, Innovative Research of America) was implanted on the lateral side of neck between the ear and the shoulder of the mice on the day before tumor cell transplantation. Water containing Doxycycline [2 mg/mL in 5% sucrose (w/v), Sigma-Aldrich] or Control (5% sucrose (w/v), Sigma-Aldrich) was administrated to each mouse cohort via bottled water supply at day 1 after tumor cell implantation. Tumor size was measured once a week with a caliper and calculated as tumor volume = Length x $Width^2$/2.

Bioluminescence Imaging, Tumor Cell Dissociation and Limiting Dilution Transplantation

Tumor bearing mice were anesthetized with isoflurane gas and given a single i.p. dose of 150 mg/kg D-luciferin (Promega) in PBS. For photon flux counting of bioluminescence, we used the IVIS Spectrum In Vivo Imaging system (PerkinElmer, Waltham, WA) coupled with a nosecone isoflurane delivery system. Results were analyzed using Living Image software provided with the IVIS imaging system. For dissociation of tumor cells grown as mouse xenografts, tumors were minced and digested with 1x collagenase/hyaluronidase (StemCell Technologies) in medium 199 (ThermoFisher Scientific), and cells were sieved sequentially through a 40 μm cell strainer (BD Falcon, USA) to obtain single cell suspension. Mouse cells were labeled with antibody against H2Kd (PE conjugated, 1:100, BD Biosciences) and gated out by flow cytometry to analyze $ALDH^+$ CSCs in $H2Kd^-$ tumor cells of human origin. For secondary transplantation, live ($DAPI^-$) $H2Kd^-$ SUM159 tumor cells sorted by FACS were prepared in 30% Matrigel (BD Biosciences) with 3 different dilutions (2500, 250 or 25 cells in 50 μl of volume for each site of injection) and injected bilaterally into the mammary fat pad (MFP) of 6-week-old female NOD/SCID mice. Tumor appearance was monitored for 3 months and frequency of tumor initiating cells following transplantation was calculated using the ELDA software (Walter + Eliza Hall Bioinformatics, Institute of Medical research).

Statistical Analysis

GraphPad Prism was used to analyze and graph data. Image J was used for image quantification. Results are presented as the mean ± standard deviation for at least three repeated individual experiments for each group. Statistical differences were determined using ANOVA or two-tailed unpaired student's t-test. A p-value of less than 0.05 was considered as statistically significant.

Results

Aberrant XIST expression promotes ALDH$^+$ E-CSCs in luminal and TN BCCs

To explore the roles of aberrant XIST expression in BCCs, we examined the relative levels of XIST expression in panels of triple negative (TN), estrogen receptor positive (ER$^+$) luminal, and HER2$^+$ BC cell lines. SUM149, a basal BC cell line derived from the inflammatory BC harboring *BRCA1* mutation (2288delT)[35] expresses minimal level of XIST (Fig. 1A). Compared to SUM149, XIST is variably expressed in a panel of TNBC cell lines, with high levels of expression found in HCC38, HCC70, MDA-MB-453, SUM159 and MDA-MD-157, while MDA-MB-468 and Vari068 modestly express, and BT20, MDA-MB-231, HCC1806 and HCC1937 BCCs express relatively low levels of XIST (Fig. 1A). Such variable XIST expression is also observed in luminal (where MCF7 expresses relatively higher level of XIST than T47D and ZR75-1) and HER2$^+$ (where BT474 and SKBR3 express relatively higher levels of XIST than HCC1954) BCCs.

To investigate the functional significance of aberrant XIST expression in luminal and TN BCCs, which contain relatively low and high proportions of E- and M-CSCs respectively, we established DOX inducible XIST KD cell lines in MCF7, a luminal BC cell line with relatively high XIST expression, and HCC70 and SUM159, two TNBC cell lines representing the basal and mesenchymal subtypes of BC respectively with high XIST expression (Fig. 1A). By quantitative real-time PCR (qRT-PCR) analysis, we confirmed that DOX-induced XIST KD in MCF7 (Fig. 1B), HCC70 (Fig. 1C) and SUM159 (Fig. 1D) significantly reduced XIST expression compared to the cells expressing a scrambled sequence (SCR). DOX-induced XIST KD modestly inhibited cell growth of MCF7 (Fig. 1E), HCC70 (Fig. 1F) and SUM159 (Fig. 1G) BCCs grown under 2D adherent conditions as evaluated by MTT assays. However, under 3D soft-agar culturing conditions, DOX-induced XIST KD markedly impaired colony-forming capacity of MCF7 and SUM159 BCCs (Fig. 1H).

We next measured tumorsphere formation at clonal density, a property of CSCs, in MCF7 and SUM159 BCCs with or without XIST KD. To ensure spheroid formation at clonal density, live (DAPI$^-$) MCF7 and SUM159 BCCs expressing shXIST hairpin vs. a SCR sequence were FACS sorted at 20 (for MCF7) or 10 (for SUM159) cells/well into ultralow-attachment 96-well plates preloaded with serum-free mammosphere medium containing DOX (1µg/ml). MCF7 (Fig. 1I and J) and SUM159 (Fig. 1I and K) BCCs exhibited significantly reduced sphere-forming capacity following DOX-induced XIST KD, suggesting that XIST expression is required to maintain self-renewal and/or proliferative capacity of

CSCs in serum-free, anchorage-independent conditions. Enumeration of $ALDH^+$ BCSCs by ALDEFLOUR assay in MCF7 (Fig. 1L), HCC70 (Fig. 1M) and SUM159 (Fig. 1N) BCCs revealed that DOX-induced XIST KD significantly decreased the proportion of $ALDH^+$ E-CSCs in each cell line, suggesting that XIST is required to maintain the proliferative $ALDH^+$ E-CSCs in luminal and TN BC.

To rule out potential off-target effects associated with a single shXIST hairpin sequence, we employed additional lentiviral vectors expressing three different DOX-inducible shXIST hairpins (shXIST-7769, shXIST-1017, shXIST-1352). DOX-induced KD of XIST in SUM159 BCCs with three distinct shXIST hairpins all significantly decreased XIST expression compared to the cells expressing a SCR sequence (Fig. S1A). Further analysis of SUM159 cells expressing shXIST-7769 vs. SCR confirmed that DOX-induced XIST KD significantly reduced the percentage of $ALDH^+$ CSCs (Fig. S1B**)**. XIST KD with shXIST-7769 vs. SCR also impairs tumorsphere-forming capacity, exemplified by significantly decreased number of spheroids formed and smaller spheroid sizes (Fig. S1C-E**)**. Together, these studies indicate that XIST promotes CSC activity and DOX-induced XIST KD significantly reduces $ALDH^+$ E-CSCs in BCCs derived from luminal and basal/mesenchymal BC.

XIST is required to maintain $CD24^{-/lo}CD44^{+/hi}$ M-CSCs in TNBC by suppressing luminal differentiation

Given a role of XIST in promoting the proliferative $ALDH^+$ E-CSCs in luminal and TN BCCs, we next examined whether aberrant XIST expression is required to maintain the more quiescent M-like CSCs characterized by $CD24^{-/lo}CD44^{+/hi}$ expression [9]. DOX-induced XIST KD in MCF7 luminal BCCs did not significantly affect the percentage of $CD24^{-/lo}CD44^{+/hi}$ M-like CSCs (Fig. S1F-H). However, in HCC70 (Fig. S1I-L) and SUM159 (Fig. S1M-P) BCCs, DOX-induced XIST KD significantly decreased the percentage of $CD24^{-/lo}CD44^{+/hi}$ M-CSC-like population compared to the cells expressing a SCR sequence. This reduction of M-CSC-like cells is mainly attributed to the significantly increased population of cells expressing epithelial marker CD24 ($CD24^+CD44^+$) in HCC70 (Fig. S1L) and SUM159 (Fig. S1P) upon DOX-induced XIST KD. This suggests that XIST inhibits luminal differentiation in TNBC cells. Together, our studies demonstrate that high XIST expression plays a role in promoting the proliferative, $ALDH^+$ E-CSCs in both luminal and TNBC. This high XIST expression is also required to maintain $CD24^{-/lo}CD44^{+/hi}$ M-CSCs in TNBC by preventing luminal differentiation.

DOX-induced XIST KD significantly abrogates tumor growth and tumor-initiating potential in xenograft models of luminal and TN BC

To determine if DOX-induced KD of XIST affects tumor growth *in vivo*, we injected SUM159 and MCF7 BCCs harboring DOX-inducible shXIST hairpin sequence (V2THS_92229) into the #4 mammary fat pad (MFP) of 6-8-week-old female NOD/SCID mice, which were randomized in two cohorts (n = 5 per cohort)

and fed with or without DOX-containing water for 11 weeks, starting one day after tumor cell injection. As shown in Fig. 2A, mice implanted with SUM159_shXIST cells without DOX treatment (Control) started to generate palpable mammary tumors at week 4 post injection, which grew rapidly to reach a mean tumor volume of 336.45 ± 120.27 mm^3 (Mean ± SD) at week 11. In contrast, mice fed with DOX-containing water for 11 weeks exhibited markedly reduced tumor growth, with a mean tumor volume of 15.52 ± 11.46 mm^3 (Mean ± SD) at week 11. Notably, following DOX withdrawal after week 11, SUM159_shXIST tumor cells resumed rapid tumor growth, suggesting that DOX-induced XIST KD did not kill SUM59 tumor cells, but rather impaired their growth potential. Similar results were observed in NOD/SCID mice implanted with MCF7_shXIST BCCs (Fig. 2B), where the mice subjected to 11-week DOX treatment displayed significantly inhibited tumor growth vs. controls, while DOX withdrawal after week 11 resulted in resumption of rapid tumor growth. This DOX-induced tumor growth retardation is not due to the direct effect of DOX, as this drug had no effect on tumor growth of parental SUM159 (Fig. S2A) or MCF7 (Fig. S2B) xenografts.

To further substantiate the role of XIST in regulating tumor growth and CSC activity, we implanted SUM159-shXIST cells with stable expression of firefly luciferase into NOD/SCID mice and monitored mammary tumor growth by bioluminescence imaging in mice fed with or without DOX-containing water. We observed a similar inhibitory effect on tumor growth upon DOX-induced XIST KD, assessed by luciferase-elicited bioluminescence imaging (Fig. 2C) and measurement of tumor volume (Fig. S2C) following DOX vs. control water treatment. Furthermore, tumors isolated from DOX-treated XIST KD mice at the end of treatment contained substantially reduced percentage of $ALDH^+$ cells compared to the tumors of control mice (Fig. 2D and E), suggesting a role of XIST in maintaining $ALDH^+$ CSCs *in vivo*.

To directly assess the impact of XIST KD on tumor-initiating potential, we performed serial dilution transplantation using $H2Kd^-$ tumor cells dissociated from SUM159 XIST KD or Control tumors into secondary NOD/SCID mice and calculated tumor initiating frequency based on subsequent tumor growth without DOX treatment. This assay revealed that DOX-induced XIST KD in primary tumor cells resulted in a 6-fold decrease in tumor initiation frequency (Fig. 2F) and significantly reduced tumor growth upon implantation of 2500 (Fig. S2D) or 250 (Fig. S2E) tumor cells .These *in vivo* studies confirmed that loss of XIST in MCF7 and SUM159 BCCs suppresses tumor growth and tumorigenic potential, presumably due to the depletion of proliferative $ALDH^+$ E-CSCs in MCF7 (Fig. 1L) and E- (Fig. 2D and E) and M-CSCs (Fig. S1M-P) in SUM159.

XIST is a master regulator of cytokine-cytokine receptor interactions

To explore the potential mechanisms by which XIST regulates tumor growth and CSC activity, we FACS sorted $ALDH^-$ and $ALDH^+$ cells from DOX-untreated SUM159-shXIST cells, which were replated and treated with or without DOX for 3 days and subjected to next-generation RNA sequencing (RNAseq). Using DOX-untreated samples as controls, we characterized the significantly downregulated ($log_2FC \leq 0.5$, blue dots) and upregulated ($log_2FC \geq 0.5$, red dots) genes in $ALDH^-$ (Fig. 3A) and $ALDH^+$ (Fig. 3B) cells upon

DOX-induced XIST KD, with data presented as volcano plots. These genes represent 22 and 23 signaling pathways significantly changed in $ALDH^-$ (Fig. 3C) and $ALDH^+$ (Fig. 3D) cells, respectively. Interestingly, in both $ALDH^-$ and $ALDH^+$ BCCs, cytokine-cytokine receptor interaction emerged as the most significantly affected pathway upon DOX-induced XIST KD.

Further heatmap analysis and mapping of the significantly changed genes involved in cytokine-cytokine receptor interaction mediated by the CXC or CC chemokine subfamilies, gp130 (IL6ST) or IL-3RB (CSFRB) shared hematopoietins, and PDGF, TNF, and TGFβ families in $ALDH^-$ (Fig. S3A) and $ALDH^+$ (Fig. S3B) BCCs revealed that a variety of proinflammatory cytokine/chemokine genes with tumor supportive functions including *IL-6*[16, 17], *IL-8* [19], *IL-1A/B*[36], *LIF* (leukemia inhibitory factor) [37], *CSF3*[38], *CXCL2*[39], *CXCL3*[40], etc. are significantly downregulated, whereas the cytokine or chemokine genes with tumor suppressive properties including *CCL5*[41], *IL-7*[42], *IL-15*[42, 43], *IL-18*[43, 44], etc. are significantly upregulated upon XIST knockdown. These unbiased RNAseq analyses suggests that aberrant XIST expression functions as a master regulator augmenting pro-inflammatory and suppressing anti-inflammatory cytokine signaling to enhance CSC activity, tumor growth and progression.

IL-6, but not IL-8, plays a prominent role mediating XIST regulation of $ALDH^+$ E-CSCs

To elucidate the significantly changed genes and pathways shared by $ALDH^-$ and $ALDH^+$ BCCs or differentially expressed in $ALDH^+$ CSCs upon DOX-induced XIST KD, we next performed Venn Diagram meta-analysis, which identified 2353 genes shared in $ALDH^-$ and $ALDH^+$ BCCs and 825 genes in $ALDH^+$ CSCs (Fig. 4A, upper panel). These genes represent 13 and 10 signaling pathways respectively (Fig. 4A, lower panel), and cytokine-cytokine receptor interaction remains as the most significantly changed pathway in $ALDH^-$ and $ALDH^+$ cells upon XIST KD (Fig. S4A). Further examination of top 25 downregulated genes in $ALDH^-$ vs. $ALDH^+$ cells upon XIST KD identified *IL-6* and *IL-8* as the top two genes most significantly inhibited in $ALDH^-$ bulk tumor cells, and these two cytokine genes are also downregulated, to a lesser extent, in $ALDH^+$ CSCs (Fig. 4B). As $ALDH^-$ BCCs represent the majority of tumor cells in the tumor mass, these data suggest that loss of XIST in BCCs significantly reduced the production of proinflammatory cytokine IL-6 and IL-8 in the tumor milieu, which may be responsible for the impaired CSC activities. We also examined the 825 significantly changed genes differentially expressed in $ALDH^+$ CSCs (Fig. 4A, upper panel), which identified *S100P* and *S100A9* as the top two genes most significantly inhibited in $ALDH^+$ CSCs but not $ALDH^-$ bulk tumor cells upon XIST KD (Fig. S4B). This suggests that S100P/A9 inflammatory proteins may have cell-autonomous roles mediating XIST regulation of $ALDH^+$ CSCs.

To validate if DOX-induced XIST KD indeed affect gene expression of *IL-6*, *IL-8*, *S100P* and *S100A9* in luminal and TN BCCs, we next performed qRT-PCR analysis of these genes in DOX-treated SUM159, HCC70 and MCF7 BCCs expressing shXIST vs. a SCR sequence. These studies confirmed the RNAseq data indicating that *IL-6* and *IL-8* gene expression are significantly and consistently inhibited in different

subtypes of BCCs upon DOX-induced XIST KD (Fig. 4C-E). Therefore, aberrant XIST expression in BCCs may promote $ALDH^+$ CSCs through IL-6 or IL-8 mediated proinflammatory signaling, which has been implicated in the regulation of CSCs, metastasis, and therapeutic resistance[17–19].

Further validation of *S100P* and *S100A9* gene expression revealed that, upon DOX-induced XIST KD, *S100P* and *S100A9* are both significantly downregulated in SUM159 (Fig. S4C), but not MCF7 (Fig. S4D) BCCs. In HCC70, DOX-induced XIST KD significantly reduces *S100P* but not *S100A9* expression (Fig. S4E). This cell-specific inhibition of *S100P/A9* expression upon DOX-induced XIST KD suggests that S100P/A9 inflammatory proteins play more significant roles in TN than in luminal BCCs to mediate XIST regulation of $ALDH^+$ CSCs.

The findings that *IL-6* and *IL-8* gene expression are consistently downregulated in MCF7, HCC70 and SUM159 BCCs following XIST KD prompted us to explore the functional significance of IL-6 and IL-8 cytokines in mediating XIST regulation of CSC activity. To do so, we tested whether exogenous IL-6 or IL-8 rescues the impaired sphere-forming capacity of SUM159 and MCF7 BCCs upon XIST KD. While 50ng/ml exogenous IL-6 had no significant impact on spheroid-forming capacity of DOX-treated SUM159 and MCF7 cells expressing a SCR sequence (Fig. S5A and B), addition of IL-6 significantly rescued spheroid-forming capacity of DOX-treated SUM159-shXIST and MCF7-shXIST BCCs (Fig. 4F-H). In contrast, addition of IL-8 at 50ng/ml failed to significantly rescue spheroid-forming capacity of SUM159 BCCs with XIST KD (Fig. S5C). This suggests that IL-6, but not IL-8, plays a prominent role mediating XIST regulation of CSC activity. Indeed, addition of IL-6 at 50ng/ml to DOX-treated SUM159-shXIST BCCs grown in 2D adherent culturing conditions for 3 days significantly rescued the decreased proportion of $ALDH^+$ CSCs, while $ALDH^+$ CSCs in SUM159 BCCs expressing a SCR sequence only had a small but not significant increase following IL-6 treatment (Fig. 4I). Similar results were obtained in HCC70 (Fig. 4J) and MCF7 (Fig. 4K), where addition of IL-6 to DOX-induced XIST KD cells significantly rescued the decreased proportion of $ALDH^+$ CSCs, while addition of IL-6 to DOX-treated cells expressing a SCR sequence had no significant effect. These data further confirm a functional role of IL-6 in mediating XIST regulation of $ALDH^+$ CSCs in luminal and TNBC. Moreover, XIST-driven IL-6 cytokine production from the bulk tumor cells appears to be sufficient in maintaining $ALDH^+$ CSCs, as exogenous IL-6 added to MCF7, HCC70 and SUM159 without XIST KD failed to significantly increase the proportion of $ALDH^+$ CSCs in each cell line.

We next examined whether exogenous IL-6 rescues the decreased proportion of $CD24^{lo}CD44^{hi}$ M-like CSCs in SUM159 BCCs with XIST KD. DOX-treated SUM159-shXIST cells incubated with IL-6 (50ng/ml) for 3 days did not exhibit significantly increased $CD24^{lo}CD44^{hi}$ M-like CSCs, although IL-6 treatment modestly but significantly increased $CD24^{lo}CD44^{hi}$ M-like CSCs in DOX-treated SUM159 BCCs expressing a SCR sequence (Fig. S5D). This suggests that loss of $CD24^{lo}CD44^{hi}$ M-like CSCs (due to increased CD24 expression and luminal differentiation) following DOX-induced XIST KD in SUM159 is not attributed to impaired IL-6 protein expression. Together, our studies support a specific role of XIST-driven IL-6 expression in maintaining $ALDH^+$ E- but not $CD24^{lo}CD44^{hi}$ M-like CSCs.

Regulation of IL-6 expression by XIST is mediated by its suppression of let-7a-2-3p

Recent studies have indicated that XIST functions as a competing endogenous RNA (ceRNA) or sponge for a large number of miRNAs [27–29]. To identify potential miRNAs directly targeted by XIST, $ALDH^-$ and $ALDH^+$ BCCs from DOX-untreated SUM159-shXIST cells were sorted, replated, and treated with or without DOX for 3 days, and subjected to GeneChip™ miRNA Array analysis. As loss of XIST de-represses its target miRNAs, we extracted the significantly upregulated miRNAs in $ALDH^-$ and $ALDH^+$ BCCs (log2 FC ≥ 0.5) treated with DOX vs. CTL. This identified 467 and 254 significantly upregulated miRNAs in $ALDH^-$ (Table S3) and $ALDH^+$ (Table S4) BCCs upon XIST KD. Meta-analysis of these two sets of miRNAs with XIST target miRNAs (Table S5) predicted by the LNCipedia database (https://lncipedia.org/) revealed 11 potential XIST targeted miRNAs that were significantly upregulated in both $ALDH^-$ bulk tumor cells and $ALDH^+$ CSCs upon XIST KD (Fig. 5A). Interestingly, let-7a-2-3p, a let-7 family of miRNAs, is markedly upregulated in $ALDH^-$ and, to a lesser extent, in $ALDH^+$ BCCs upon XIST KD (Fig. 5B). As let-7 miRNAs including let-7a directly repress IL-6 cytokine production in breast epithelial cells[17], these data suggest a role of XIST by repressing let-7a-2-3p in $ALDH^-$ bulk tumor cells to increase IL-6 production, which in turn promotes $ALDH^+$ CSCs. qRT-PCR validation of let-7a-2-3p in SUM159, HCC70 and MCF7 BCCs confirmed that let-7a-2-3p is consistently upregulated following DOX-induced XIST KD (Fig. 5C), suggesting an important role of XIST in repressing let-7a-2-3p across different subtypes of BCCs.

In addition to let-7a-2-3p, we also validated 10 other potential miRNA targets of XIST (Fig. 5B). qRT-PCR analyses of DOX-treated SUM159-shXIST vs. SCR cells confirmed that miR-374b-5p, miR-181c-5p and miR-1303 are significantly upregulated, while the rest of miRNAs were not significantly changed upon XIST KD (Fig. S5E). This suggests that miR-374b-5p, miR-181c-5p and miR-1303 may serve as additional miRNA targets mediating XIST regulation of IL-6 expression and $ALDH^+$ CSCs.

We next investigated whether introduction of miRNA inhibitors (antagomirs) against let-7a-2-3p, miR-374b-5p, miR-181c-5p and miR-1303 rescues the reduced *IL-6* gene expression in BCCs subjected to DOX-induced XIST KD. Transfection of a let-7a-2-3p inhibitor vs. a negative control sequence (N.C.) into DOX-treated SUM159-shXIST (Fig. S6A), HCC70-shXIST (Fig. S6B) and MCF7-shXIST (Fig. S6C) BCCs all significantly inhibited let-7a-2-3p expression, leading to significantly increased *IL-6* gene expression in each XIST KD cell line (Fig. 5D). This confirms that let-7a-2-3p serves as a specific miRNA targeted by XIST to promote IL-6 protein expression in different subtypes of BCCs. Introduction of miRNA inhibitors against miR-374b-5p, miR-181c-5p or miR-1303 vs. N.C. into DOX-treated SUM159-shXIST BCCs significantly inhibited the expression of each corresponding miRNA (Fig. S6D-F). However, these specific miRNA inhibitors failed to significantly increase *IL-6* gene expression (Fig. S6G and H) and the proportion of $ALDH^+$ CSCs (Fig. S6I and J). Thus, let-7a-2-3p, but not miR-374b-5p, miR-181c-5p and miR-1303, is the specific miRNA targeted by XIST to promote IL-6 protein expression.

Molecular mapping of functional let-7a-2-3p binding sites in XIST

To characterize the specific XIST sequences that interact with let-7a-2-3p, we employed the TargetScan database to search for potential let-7a-2-3p binding sites in XIST, which identified two predicted sites (Site 1 and Site 2) with highest probability of binding let-7a-2-3p (Fig. 5E and F). To determine the functional significance of these two XIST sites for interaction with let-7a-2-3p, we cloned the corresponding XIST cDNA fragment containing Site 1 or Site 2 (Table S2) into the PmirGLO dual-luciferase miRNA target expression vector, and subsequently transfected these constructs into SUM159 BCCs to evaluate the capacity of these XIST fragments to suppress luciferase reporter activity when co-transfected with a let-7a-2-3p mimic vs. control RNA (ctrl). Although introduction of let-7a-2-3p mimic vs. ctrl into SUM159 BCCs markedly boosted let-7a-2-3p expression (Fig. 5G), let-7a-2-3p mimic selectively inhibited luciferase reporter activity of SUM159 BCCs expressing the luciferase reporter plasmid containing Site 2 (Fig. 5I), but not Site 1 (Fig. 5H). This suggests that Site 2 serves as a functional region of XIST to interact with let-7a-2-3p, leading to the suppression of luciferase reporter activity. Further site-directed mutagenesis of Site 2 (Fig. 5F, lower panel) abolished let-7a-2-3p mimic induced suppression of luciferase reporter activity (Fig. 5I), confirming that Site 2 of XIST acts as a functional region mediating its repression of let-7a-2-3p, leading to increased IL-6 production in BCCs.

To determine if increased let-7a-2-3p expression in BCCs with XIST KD is responsible for the inhibition of $ALDH^+$ CSCs, we next transfected DOX-treated SUM159-shXIST, HCC70-shXIST and MCF7-shXIST BCCs with let-7a-2-3p inhibitor vs. N.C. and performed ALDEFLOUR assay three days after let-7a-2-3p inhibitor transection. Introduction of let-7a-2-3p inhibitor vs. N.C. significantly increased $ALDH^+$ CSCs in MCF7 (Fig. 5J), SUM159 (Fig. 5K) and HCC70 (Fig. S7A) BCCs with XIST KD. In contrast to BCCs harboring XIST KD, introduction of let-7a-2-3p inhibitor vs. N.C. in DOX-treated MCF7 (Fig. S7B) or SUM159 (Fig. S7C) BCCs expressing a SCR sequence failed to significantly increase $ALDH^+$ CSCs. This suggests that let-7a-2-3p is repressed by XIST in MCF7 and SUM159 BCCs, rendering them refractory to let-7a-2-3p inhibitor treatment.

Given the fact that introduction of let-7a-2-3p inhibitor into different BCCs harboring DOX-induced XIST KD significantly rescues the reduced proportion of $ALDH^+$ CSCs (Fig. 5J and K and Fig. S7A), we next asked whether the let-7a-2-3p inhibitor is sufficient to rescue the reduced $CD24^{lo}CD44^{hi}$ M-CSCs in HCC70 basal BCCs subjected to DOX-induced XIST KD (Fig. S1I-L). Contrary to significantly increased $ALDH^+$ E-CSCs induced by let-7a-2-3p inhibitor treatment (Fig. S7A), introduction of let-7a-2-3p inhibitor vs. N.C. in DOX-treated HCC70-shXIST cells failed to increase $CD24^{lo}CD44^{hi}$ M-CSCs (Fig. S7D). This suggests that XIST-mediated repression of let-7a-2-3p specifically regulates $ALDH^+$ E- but not $CD24^{lo}CD44^{hi}$ M-CSCs in TNBC. Together, our studies demonstrate a specific role of aberrant XIST expression in luminal and TN BCCs to repress let-7a-2-3p by acting as a ceRNA, leading to increased IL-6 cytokine production to promote $ALDH^+$ E- but not $CD24^{lo}CD44^{hi}$ M-CSCs.

XIST expression in ALDH $^{-}$ bulk tumor cells drives paracrine IL-6 signaling to activate STAT3 in ALDH^{+} cells

To investigate how XIST-driven IL-6 expression regulates ALDH^{+} CSCs, we next examined if DOX-induced XIST KD in luminal and TN BCCs affects the activation of NFkB/STAT3 signaling pathways downstream of IL-6, leading to suppressed expression of key CSC regulatory proteins. Compared to SCR control cells, SUM159-shXIST BCCs treated with DOX for 3 days displayed markedly reduced phosphorylation of STAT3 at Tyr705 (p-STAT3), while total STAT3 protein expression was not significantly changed (Fig. 6A), indicating diminished STAT3 activation upon XIST KD in SUM159 BCCs. In contrast to markedly reduced STAT3 activation, activation of the p65 NFκB, indicated by the ratio of phospho-NFκB p65 (Ser536) to total p65 NFκB, was not significantly affected following XIST KD. We also observed that c-MYC, a key CSC regulatory protein and transcriptional factor implicated in promoting tumor growth and cancer stemness, was markedly reduced in SUM159-shXIST but not SCR cells following DOX treatment (Fig. 6A). These studies suggest that DOX-induced XIST KD results in decreased tumor growth and CSC activity by impairing STAT3 activation and c-MYC expression.

To further explore potential changes in the expression of other CSC-regulatory proteins upon DOX induced XIST KD, we cultivated tumorspheres using SUM159-shXIST and MCF-shXIST as well as corresponding SCR cells in the absence or presence of DOX for 14 days. Consistent with reduced STAT3 activation in DOX-treated SUM159-shXIST cells grown under 2D adherent conditions (Fig. 6A), significantly reduced STAT3 activation was also observed in tumorsphere lysates derived from DOX-treated SUM159-shXIST (Fig. 6B) and MCF-shXIST (Fig. 6C) cells. Further immunoblotting with specific antibodies against CSC regulatory factors including SOX2, SOX9, OCT4 and KLF4 revealed that KLF4 expression was consistently suppressed in DOX-treated SUM159-shXIST (Fig. 6B) and MCF-shXIST (Fig. 6C) spheroid cells, whereas SOX2 and OCT4 expression were not significantly changed. We also found that SOX9, which is expressed in luminal MCF7 but not mesenchymal SUM159 BCCs, was markedly suppressed upon DOX-induced XIST KD in MCF7 tumor spheroids (Fig. 6C). Therefore, DOX-induced XIST KD in luminal and TN BCCs blunted IL-6 mediated STAT3 activation, leading to impaired expression of key CSC regulatory factors including c-MYC, KLF4 and SOX9.

Our RNAseq analyses indicated *IL-6* as the gene most significantly inhibited in ALDH^{-} bulk tumor cells upon XIST KD, although this gene is also downregulated in ALDH^{+} CSCs (Fig. 4B). In parallel with the most significant inhibition of *IL-6* expression in ALDH^{-} bulk tumor cells, miRNA array analysis unveiled that let-7a-2-3p is more robustly upregulated in ALDH^{-} BCCs vs. ALDH^{+} CSCs following XIST KD (Fig. 5B). To understand how XIST-driven IL-6 production in ALDH^{-} BCCs affects ALDH^{+} CSCs, we hypothesize that ALDH^{+} CSCs have preferential responses to IL-6 due to their elevated expression of IL6R compared to ALDH^{-} BCCs. To test this idea, we sorted ALDH^{+} CSCs and ALDH^{-} BCCs from SUM159 and performed qRT-PCR analysis to determine their relative expression of *IL6R* and *IL6ST*, the latter of which encodes the IL-6 cytokine family signal transducer or gp130. Indeed, ALDH^{+} CSCs express significantly higher levels of

IL6R (Fig. 6D) compared to ALDH$^-$ BCCs. In contrast to *IL6R*, *IL6ST* expression is not significantly different between ALDH$^-$ and ALDH$^+$ BCCs (Fig. 6E). Based on these findings, we present a model to illustrate the mechanism of XIST regulating ALDH$^+$ CSCs in BC. In this model, aberrantly expressed XIST in ALDH$^-$ bulk tumor cells sequesters let-7a-2-3p in the nucleus, blocking its repression of IL-6 protein expression. This XIST-driven production of IL-6 from ALDH$^-$ bulk tumor cells preferentially binds to IL6R on ALDH$^+$ CSCs to drive STAT3 activation and the expression of key CSC factors (i.e., c-MYC, KLF4 and SOX9), promoting self-renewal of ALDH$^+$ CSCs (Fig. 7). Although IL-6 produced from ALDH$^-$ bulk tumor cells promotes ALDH$^+$ CSCs in a paracrine fashion, downregulation of *IL-6* (Fig. 4B) and upregulation of let-7a-2-3p (Fig. 5B) expression, despite to a lesser extent, were also detected in ALDH$^+$ CSCs upon XIST KD. As let-7 miRNAs are mainly expressed in bulk tumor cells but not breast CSCs [34], we think XIST-driven IL-6 production from ALDH$^-$ bulk tumor cells plays a major role in maintaining ALDH$^+$ CSCs via paracrine IL-6 signaling.

Discussion

As one of the best studied lncRNAs, XIST functions as a master regulator of XCI during early embryogenesis in female mammals. However, in post-XCI somatic tissues, dysregulation of XIST has recently been documented to play a role in chronic inflammatory diseases such as atherosclerosis[45], coronary artery disease[46], myocardial infarction[47], Alzheimer's disease[48], Parkinson disease[49], among others. Aberrant expression of XIST also promotes inflammatory responses during tissue injury such as cerebral ischemia/reperfusion injury[50], lipopolysaccharide (LPS)-induced acute lung injury (ALI) [51], and sepsis-induced acute liver injury[52]. In parallel with dysregulated XIST expression in post-XCI somatic tissues, aberrant expression of XIST in post-XCI BC cells is a common phenomenon implicated in therapeutic resistance by regulating breast CSCs [30–32]. Despite previous studies demonstrating a link of aberrant XIST expression to inflammation and cancer stemness, the mechanisms involved remain elusive.

Using unbiased RNAseq analysis, we discovered that DOX-inducible XIST KD in SUM159 ALDH$^-$ bulk tumor cells and ALDH$^+$ CSCs most significantly altered the cytokine-cytokine receptor interaction pathways in each cell population, leading to pronounced suppression of proinflammatory cytokines IL-6 and IL-8. As IL-6 and IL-8 act as key regulators of tumor progression and CSC activity[16, 17, 19], we focused on IL-6 and IL-8 in this study to determine their roles in mediating XIST regulation of ALDH$^+$ E-CSCs. Although both *IL-6* and *IL-8* gene expression were consistently downregulated in luminal MCF7 as well as SUM159 and HCC70 TN BCCs following DOX-induced XIST KD, we found IL-6, but not IL-8, plays a dominant role in mediating XIST regulation of ALDH$^+$ E-CSCs. We further demonstrated that XIST promotes the proliferative, ALDH$^+$ E-CSCs in luminal and TN BCCs by derepressing let-7 controlled paracrine IL-6-STAT3 signaling to increase the expression of CSC-associated factors including c-MYC, KLF4 and SOX9, promoting self-renewal of ALDH$^+$ E-CSCs.

In addition to suppressing the expression of tumor supportive cytokines such as IL-6, IL-8, IL1A/B, LIF, G/M-CSF, DOX-induced KD of XIST also enhances the expression of tumor suppressive cytokines such as IL-7, IL-15, IL-18, etc., suggesting that XIST functions as a master regulator of cytokine-cytokine receptor interactions, leading to increased tumor growth and CSC activity. Future studies will be necessary to define the functional significance and underlying mechanisms of other tumor supportive cytokines/chemokines (i.e., IL1A/B, LIF, G/M-CSF and CXCL2/3) and inflammatory proteins (i.e., S100P and S100A9) in mediating XIST regulation of tumor growth and CSC activity. Similarly, the functional relevance and mechanisms of XIST in inhibiting tumor suppressive cytokine/chemokines (i.e., IL-7, IL-15, and IL-18) need to be determined.

In this study, we elucidated the mechanisms of XIST regulating IL-6 expression and $ALDH^+$ CSCs, focusing on potential miRNAs targeted by XIST via its molecular sponge function. Through unbiased miRNA array analysis, we discovered that let-7a-2-3p, a member of let-7 tumor suppressor miRNAs known to repress IL-6 cytokine production [17, 33], is markedly upregulated in $ALDH^-$ bulk tumor cells upon DOX-induced XIST KD. We systematically validated this upregulated let-7a-2-3p expression in SUM159, HCC70 and MCF7 BCCs following XIST KD, and subsequently verified the functional relevance of this upregulated let-7a-2-3p in suppressing *IL-6* gene expression and maintenance of $ALDH^+$ CSCs. Lastly, we utilized luciferase reporter assay to define the regions of XIST that specifically interact with let-7a-2-3p, leading to activation of IL-6 protein expression.

In addition to acting as a major molecular sponge to antagonize many different regulatory ncRNAs, XIST also functions as a macromolecular scaffold for protein recruitment and acts as cis regulatory elements to modulate gene transcription, RNA splicing and post-transcriptional modification [53–56]. For instance, XIST mediates the recruitment of polycomb repressive complex (PRC) 1 and 2 to participate in XCI, leading to chromosome-wide gene silencing [57, 58]. In this study, we discovered that DOX-induced KD of XIST in HCC70 and SUM159 basal/mesenchymal, but not MCF7 luminal BCCs, significantly abrogated $CD24^{lo}CD44^{hi}$ M-CSCs by promoting CD24 epithelial marker expression (Fig. S1F-P). This suggests a role of XIST in repressing luminal differentiation in TNBC by silencing CD24 expression. Future studies will be necessary to clarify if and how XIST functions to recruit PRC1/2 and other epigenetic modifiers to silence CD24 expression and maintain $CD24^{lo}CD44^{hi}$ M-CSCs in TNBC.

One intriguing phenomena for XIST is that its expression is markedly variable across different BC cells, even those derived from the same subtype (i.e., basal/luminal) of BC. This suggests that XIST expression in BC is regulated in a context-dependent manner. Intriguingly, it was reported that the Xi is lost in all examined BC cell lines regardless of *BRCA1* status, and that XIST in BCCs may be transcribed from the Xa, which exist in more than one copy [24]. Therefore, aberrant XIST expression in BCCs may play functional roles totally unrelated to XCI. As abnormal expression of XIST has been shown to associate with poor prognosis in patients with different cancer types, including BC [59, 60], pancreatic cancer [61], colorectal cancer [62] and brain cancer [63], this pathological roles of XIST in driving tumor growth and progression may relate to its multifaceted functions by acting as a molecular sponge to repress a number

of tumor suppressor ncRNAs, and by recruiting epigenetic modifiers to alter chromatin structure and accessibility [21].

The mechanisms underlying dysregulation of XIST in BC and other malignancies remain elusive. Emerging evidence suggests that XIST and STAT3, by mutually regulating each other, form a double positive feedback loop that promotes inflammation and cancer development. XIST, by sponging/antagonizing miR-124, a STAT3 targeting miRNA, enhances STAT3 expression in retinoblastoma[64]. In LPS-induced ALI, XIST functions as a molecular sponge of miR-146a-5p positively regulating STAT3, which is then recruited to the promoter region of XIST to accelerate its transcription, thereby constituting a positive feedback loop that promotes inflammatory responses in ALI[51]. We suggest that this double positive feedback loop of XIST and STAT3 may contribute to the dysregulation of XIST in BC and other tumor types. This mutual regulation of XIST and STAT3 further supports a role of XIST in promoting cancer stemness.

Conclusions

In summary, our study unveiled a novel role of XIST in promoting $ALDH^+$ CSCs in luminal and TN BC by antagonizing let-7a-2-3p in bulk tumor cells to enhance IL-6 production, which preferentially binds to IL6R on $ALDH^+$ CSCs to drive STAT3 activation and c-MYC, KLF4 and SOX9 expression, promoting self-renewal of $ALDH^+$ CSCs (Fig. 7). In addition to a universal role in promoting $ALDH^+$ E-CSCs, XIST is also required to maintain $CD24^{-/lo}CD44^{+/hi}$ M-CSCs in basal/mesenchymal BCCs by inhibiting luminal differentiation, and this function is independent of its suppression of let-7a-2-3p. As DOX-induced XIST KD markedly abrogates tumor growth and CSC activities across different subtypes of BC, our study also identifies XIST as a potential therapeutic target for CSCs in BC and other malignancies.

Abbreviations

ALDH
aldehyde dehydrogenase
ALI
Acute lung injury
BC
breast cancer
BCCs
breast cancer cells
BRCA1
Breast cancer gene 1
CSCs
cancer-stem like cells
DOX

Doxycycline
HDACi
histone deacetylase inhibitors
KD
knockdown
IL-6
Interleukin-6
IL6R
IL-6 receptor
IL6ST
IL-6 cytokine family signal transducer
lncRNA
long noncoding RNA
LPS
lipopolysaccharide
MFP
Mammary fat pad
NFκB
Nuclear factor κB
PRC
Polycomb repressive complex
RNAseq
next-RNA sequencing
STAT3
Signal transducer and activator of transcription 3
TNBC
Triple negative breast cancer
Xa
Active X chromosome
XCI
X chromosome inactivation
Xi
Inactive X chromosome
XIST
X-inactive specific transcript.

Declarations

Acknowledgements

We thank UM Flow Cytometry core for assistance in flow analysis and sorting and Drs. Grace Bushnell and Deeksha Sharma for editing this manuscript. This research was supported by R35CA197585 from the NIH and BCRF-21-173 from the Breast Cancer Research Foundation to MSW and ML, and NIH R01GM118928 to JL.

Authors' contributions

Y.M., Y.Z. and M.L. designed and executed this study. M.L. wrote the manuscript. M.S.W. reviewed experimental data and edited the manuscript. L.S. performed cell culture, FACS analysis and sorting as well as qRT-PCR and animal studies. Y.Q. and N.S. helped with cell culture and animal experiments, Q.S. and J.L. with RNAseq and bioinformatics analysis.

Availability of data and material

All of the data and material in this paper are available when requested.

Ethics approval and consent to participate

All animal studies conducted in this study were reviewed and approved by the Institutional Animal Care and Use Committee (IACUC) at the University of Michigan. This study does not involve human subjects.

Consent for publication

All authors agree to the content of the manuscript and to publish the manuscript as co-authors.

Competing interests

The authors declare no potential conflicts of interest.

References

1. Luo M, Clouthier SG, Deol Y, Liu S, Nagrath S, Azizi E, Wicha MS: **Breast cancer stem cells: current advances and clinical implications**. Methods Mol Biol 2015, **1293**:1–49.
2. Liu S, Wicha MS: **Targeting breast cancer stem cells**. J Clin Oncol 2010, **28**:4006–4012.
3. Ginestier C, Hur MH, Charafe-Jauffret E, Monville F, Dutcher J, Brown M, Jacquemier J, Viens P, Kleer CG, Liu S, et al: **ALDH1 is a marker of normal and malignant human mammary stem cells and a predictor of poor clinical outcome**. Cell Stem Cell 2007, **1**:555–567.
4. Huang EH, Hynes MJ, Zhang T, Ginestier C, Dontu G, Appelman H, Fields JZ, Wicha MS, Boman BM: **Aldehyde dehydrogenase 1 is a marker for normal and malignant human colonic stem cells (SC) and tracks SC overpopulation during colon tumorigenesis**. Cancer Res 2009, **69**:3382–3389.
5. Cheung AM, Wan TS, Leung JC, Chan LY, Huang H, Kwong YL, Liang R, Leung AY: **Aldehyde dehydrogenase activity in leukemic blasts defines a subgroup of acute myeloid leukemia with adverse prognosis and superior NOD/SCID engrafting potential**. Leukemia 2007, **21**:1423–1430.

6. Kim MP, Fleming JB, Wang H, Abbruzzese JL, Choi W, Kopetz S, McConkey DJ, Evans DB, Gallick GE: **ALDH activity selectively defines an enhanced tumor-initiating cell population relative to CD133 expression in human pancreatic adenocarcinoma**. PLoS One 2011, **6**:e20636.
7. van den Hoogen C, van der Horst G, Cheung H, Buijs JT, Lippitt JM, Guzman-Ramirez N, Hamdy FC, Eaton CL, Thalmann GN, Cecchini MG, et al: **High aldehyde dehydrogenase activity identifies tumor-initiating and metastasis-initiating cells in human prostate cancer**. Cancer Res 2010, **70**:5163–5173.
8. Vassalli G: **Aldehyde Dehydrogenases: Not Just Markers, but Functional Regulators of Stem Cells**. Stem Cells Int 2019, **2019**:3904645.
9. Al-Hajj M, Wicha MS, Benito-Hernandez A, Morrison SJ, Clarke MF: **Prospective identification of tumorigenic breast cancer cells**. Proc Natl Acad Sci U S A 2003, **100**:3983–3988.
10. Liu S, Cong Y, Wang D, Sun Y, Deng L, Liu Y, Martin-Trevino R, Shang L, McDermott SP, Landis MD, et al: **Breast Cancer Stem Cells Transition between Epithelial and Mesenchymal States Reflective of their Normal Counterparts**. Stem Cell Reports 2014, **2**:78–91.
11. Lin L, Hutzen B, Lee HF, Peng Z, Wang W, Zhao C, Lin HJ, Sun D, Li PK, Li C, et al: **Evaluation of STAT3 signaling in ALDH + and ALDH+/CD44+/CD24- subpopulations of breast cancer cells**. PLoS One 2013, **8**:e82821.
12. Polyak K, Haviv I, Campbell IG: **Co-evolution of tumor cells and their microenvironment**. Trends Genet 2009, **25**:30–38.
13. Liu S, Ginestier C, Ou SJ, Clouthier SG, Patel SH, Monville F, Korkaya H, Heath A, Dutcher J, Kleer CG, et al: **Breast cancer stem cells are regulated by mesenchymal stem cells through cytokine networks**. Cancer Res 2011, **71**:614–624.
14. Korkaya H, Liu S, Wicha MS: **Regulation of cancer stem cells by cytokine networks: attacking cancer's inflammatory roots**. Clin Cancer Res 2011, **17**:6125–6129.
15. Elaraj DM, Weinreich DM, Varghese S, Puhlmann M, Hewitt SM, Carroll NM, Feldman ED, Turner EM, Alexander HR: **The role of interleukin 1 in growth and metastasis of human cancer xenografts**. Clin Cancer Res 2006, **12**:1088–1096.
16. Iliopoulos D, Hirsch HA, Wang G, Struhl K: **Inducible formation of breast cancer stem cells and their dynamic equilibrium with non-stem cancer cells via IL6 secretion**. Proc Natl Acad Sci U S A 2011, **108**:1397–1402.
17. Iliopoulos D, Hirsch HA, Struhl K: **An epigenetic switch involving NF-kappaB, Lin28, Let-7 MicroRNA, and IL6 links inflammation to cell transformation**. Cell 2009, **139**:693–706.
18. Korkaya H, Kim GI, Davis A, Malik F, Henry NL, Ithimakin S, Quraishi AA, Tawakkol N, D'Angelo R, Paulson AK, et al: **Activation of an IL6 inflammatory loop mediates trastuzumab resistance in HER2 + breast cancer by expanding the cancer stem cell population**. Mol Cell 2012, **47**:570–584.
19. Ginestier C, Liu S, Diebel ME, Korkaya H, Luo M, Brown M, Wicinski J, Cabaud O, Charafe-Jauffret E, Birnbaum D, et al: **CXCR1 blockade selectively targets human breast cancer stem cells in vitro and in xenografts**. J Clin Invest 2010, **120**:485–497.

20. Brown CJ, Ballabio A, Rupert JL, Lafreniere RG, Grompe M, Tonlorenzi R, Willard HF: **A gene from the region of the human X inactivation centre is expressed exclusively from the inactive X chromosome**. Nature 1991, **349**:38–44.
21. Giorgetti L, Lajoie BR, Carter AC, Attia M, Zhan Y, Xu J, Chen CJ, Kaplan N, Chang HY, Heard E, Dekker J: **Structural organization of the inactive X chromosome in the mouse**. Nature 2016, **535**:575–579.
22. Yildirim E, Kirby JE, Brown DE, Mercier FE, Sadreyev RI, Scadden DT, Lee JT: **Xist RNA is a potent suppressor of hematologic cancer in mice**. Cell 2013, **152**:727–742.
23. Richart L, Picod-Chedotel ML, Wassef M, Macario M, Aflaki S, Salvador MA, Hery T, Dauphin A, Wicinski J, Chevrier V, et al: **XIST loss impairs mammary stem cell differentiation and increases tumorigenicity through Mediator hyperactivation**. *Cell* 2022.
24. Sirchia SM, Ramoscelli L, Grati FR, Barbera F, Coradini D, Rossella F, Porta G, Lesma E, Ruggeri A, Radice P, et al: **Loss of the inactive X chromosome and replication of the active X in BRCA1-defective and wild-type breast cancer cells**. Cancer Res 2005, **65**:2139–2146.
25. Chaligne R, Popova T, Mendoza-Parra MA, Saleem MA, Gentien D, Ban K, Piolot T, Leroy O, Mariani O, Gronemeyer H, et al: **The inactive X chromosome is epigenetically unstable and transcriptionally labile in breast cancer**. Genome Res 2015, **25**:488–503.
26. Sirchia SM, Tabano S, Monti L, Recalcati MP, Gariboldi M, Grati FR, Porta G, Finelli P, Radice P, Miozzo M: **Misbehaviour of XIST RNA in breast cancer cells**. PLoS One 2009, **4**:e5559.
27. Yang Z, Jiang X, Jiang X, Zhao H: **X-inactive-specific transcript: A long noncoding RNA with complex roles in human cancers**. Gene 2018, **679**:28–35.
28. Chen YK, Yen Y: **The Ambivalent Role of lncRNA Xist in Carcinogenesis**. Stem Cell Rev Rep 2019, **15**:314–323.
29. Ghafouri-Fard S, Dashti S, Farsi M, Taheri M, Mousavinejad SA: **X-Inactive-Specific Transcript: Review of Its Functions in the Carcinogenesis**. Front Cell Dev Biol 2021, **9**:690522.
30. Rottenberg S, Vollebergh MA, de Hoon B, de Ronde J, Schouten PC, Kersbergen A, Zander SA, Pajic M, Jaspers JE, Jonkers M, et al: **Impact of intertumoral heterogeneity on predicting chemotherapy response of BRCA1-deficient mammary tumors**. Cancer Res 2012, **72**:2350–2361.
31. Schouten PC, Vollebergh MA, Opdam M, Jonkers M, Loden M, Wesseling J, Hauptmann M, Linn SC: **High XIST and Low 53BP1 Expression Predict Poor Outcome after High-Dose Alkylating Chemotherapy in Patients with a BRCA1-like Breast Cancer**. Mol Cancer Ther 2016, **15**:190–198.
32. Salvador MA, Wicinski J, Cabaud O, Toiron Y, Finetti P, Josselin E, Lelievre H, Kraus-Berthier L, Depil S, Bertucci F, et al: **The histone deacetylase inhibitor abexinostat induces cancer stem cells differentiation in breast cancer with low Xist expression**. Clin Cancer Res 2013, **19**:6520–6531.
33. Ma Y, Shen N, Wicha MS, Luo M: **The Roles of the Let-7 Family of MicroRNAs in the Regulation of Cancer Stemness**. Cells 2021, **10**.
34. Yu F, Yao H, Zhu P, Zhang X, Pan Q, Gong C, Huang Y, Hu X, Su F, Lieberman J, Song E: **let-7 regulates self renewal and tumorigenicity of breast cancer cells**. Cell 2007, **131**:1109–1123.

35. Elstrodt F, Hollestelle A, Nagel JH, Gorin M, Wasielewski M, van den Ouweland A, Merajver SD, Ethier SP, Schutte M: **BRCA1 mutation analysis of 41 human breast cancer cell lines reveals three new deleterious mutants**. Cancer Res 2006, **66**:41–45.
36. Gelfo V, Romaniello D, Mazzeschi M, Sgarzi M, Grilli G, Morselli A, Manzan B, Rihawi K, Lauriola M: **Roles of IL-1 in Cancer: From Tumor Progression to Resistance to Targeted Therapies**. Int J Mol Sci 2020, **21**.
37. Bian SB, Yang Y, Liang WQ, Zhang KC, Chen L, Zhang ZT: **Leukemia inhibitory factor promotes gastric cancer cell proliferation, migration, and invasion via the LIFR-Hippo-YAP pathway**. Ann N Y Acad Sci 2021, **1484**:74–89.
38. Pickup MW, Owens P, Gorska AE, Chytil A, Ye F, Shi C, Weaver VM, Kalluri R, Moses HL, Novitskiy SV: **Development of Aggressive Pancreatic Ductal Adenocarcinomas Depends on Granulocyte Colony Stimulating Factor Secretion in Carcinoma Cells**. Cancer Immunol Res 2017, **5**:718–729.
39. Taki M, Abiko K, Baba T, Hamanishi J, Yamaguchi K, Murakami R, Yamanoi K, Horikawa N, Hosoe Y, Nakamura E, et al: **Snail promotes ovarian cancer progression by recruiting myeloid-derived suppressor cells via CXCR2 ligand upregulation**. Nat Commun 2018, **9**:1685.
40. Zhang L, Zhang L, Li H, Ge C, Zhao F, Tian H, Chen T, Jiang G, Xie H, Cui Y, et al: **CXCL3 contributes to CD133(+) CSCs maintenance and forms a positive feedback regulation loop with CD133 in HCC via Erk1/2 phosphorylation**. Sci Rep 2016, **6**:27426.
41. Mowat C, Mosley SR, Namdar A, Schiller D, Baker K: **Anti-tumor immunity in mismatch repair-deficient colorectal cancers requires type I IFN-driven CCL5 and CXCL10**. J Exp Med 2021, **218**.
42. Song Y, Liu Y, Hu R, Su M, Rood D, Lai L: **In Vivo Antitumor Activity of a Recombinant IL7/IL15 Hybrid Cytokine in Mice**. Mol Cancer Ther 2016, **15**:2413–2421.
43. Ewen EM, Pahl JHW, Miller M, Watzl C, Cerwenka A: **KIR downregulation by IL-12/15/18 unleashes human NK cells from KIR/HLA-I inhibition and enhances killing of tumor cells**. Eur J Immunol 2018, **48**:355–365.
44. Saetang J, Chonpathompikunlert P, Sretrirutchai S, Roongsawang N, Kayasut K, Voravuthikunchai SP, Sukketsiri W, Tipmanee V, Sangkhathat S: **Anti-cancer effect of engineered recombinant interleukin 18**. Adv Clin Exp Med 2020, **29**:1135–1143.
45. Yang K, Xue Y, Gao X: **LncRNA XIST Promotes Atherosclerosis by Regulating miR-599/TLR4 Axis**. Inflammation 2021, **44**:965–973.
46. Sohrabifar N, Ghaderian SMH, Alipour Parsa S, Ghaedi H, Jafari H: **Variation in the expression level of MALAT1, MIAT and XIST lncRNAs in coronary artery disease patients with and without type 2 diabetes mellitus**. Arch Physiol Biochem 2020:1–8.
47. Zhou T, Qin G, Yang L, Xiang D, Li S: **LncRNA XIST regulates myocardial infarction by targeting miR-130a-3p**. J Cell Physiol 2019, **234**:8659–8667.
48. Yue D, Guanqun G, Jingxin L, Sen S, Shuang L, Yan S, Minxue Z, Ping Y, Chong L, Zhuobo Z, Yafen W: **Silencing of long noncoding RNA XIST attenuated Alzheimer's disease-related BACE1 alteration through miR-124**. Cell Biol Int 2020, **44**:630–636.

49. Sun AG, Wang J, Shan YZ, Yu WJ, Li X, Cong CH, Wang X: **Identifying distinct candidate genes for early Parkinson's disease by analysis of gene expression in whole blood**. Neuro Endocrinol Lett 2014, **35**:398–404.
50. Wang J, Fu Z, Wang M, Lu J, Yang H, Lu H: **Knockdown of XIST Attenuates Cerebral Ischemia/Reperfusion Injury Through Regulation of miR-362/ROCK2 Axis**. Neurochem Res 2021, **46**:2167–2180.
51. Li J, Xue L, Wu Y, Yang Q, Liu D, Yu C, Peng J: **STAT3-activated lncRNA XIST accelerates the in fl ammatory response and apoptosis of LPS-induced acute lung injury**. J Cell Mol Med 2021, **25**:6550–6557.
52. Shen C, Li J: **LncRNA XIST silencing protects against sepsis-induced acute liver injury via inhibition of BRD4 expression**. Inflammation 2021, **44**:194–205.
53. Pintacuda G, Young AN, Cerase A: **Function by Structure: Spotlights on Xist Long Non-coding RNA**. Front Mol Biosci 2017, **4**:90.
54. Chu C, Zhang QC, da Rocha ST, Flynn RA, Bharadwaj M, Calabrese JM, Magnuson T, Heard E, Chang HY: **Systematic discovery of Xist RNA binding proteins**. Cell 2015, **161**:404–416.
55. McHugh CA, Chen CK, Chow A, Surka CF, Tran C, McDonel P, Pandya-Jones A, Blanco M, Burghard C, Moradian A, et al: **The Xist lncRNA interacts directly with SHARP to silence transcription through HDAC3**. Nature 2015, **521**:232–236.
56. Markaki Y, Gan Chong J, Wang Y, Jacobson EC, Luong C, Tan SYX, Jachowicz JW, Strehle M, Maestrini D, Banerjee AK, et al: **Xist nucleates local protein gradients to propagate silencing across the X chromosome**. Cell 2021, **184**:6174–6192 e6132.
57. Bousard A, Raposo AC, Zylicz JJ, Picard C, Pires VB, Qi Y, Gil C, Syx L, Chang HY, Heard E, da Rocha ST: **The role of Xist-mediated Polycomb recruitment in the initiation of X-chromosome inactivation**. EMBO Rep 2019, **20**:e48019.
58. Schoeftner S, Sengupta AK, Kubicek S, Mechtler K, Spahn L, Koseki H, Jenuwein T, Wutz A: **Recruitment of PRC1 function at the initiation of X inactivation independent of PRC2 and silencing**. EMBO J 2006, **25**:3110–3122.
59. Zong Y, Zhang Y, Hou D, Xu J, Cui F, Qin Y, Sun X: **The lncRNA XIST promotes the progression of breast cancer by sponging miR-125b-5p to modulate NLRC5**. Am J Transl Res 2020, **12**:3501–3511.
60. Swellam M, El Magdoub HM, Shawki MA, Adel M, Hefny MM, El-Shazly SS: **Clinical impact of LncRNA XIST and LncRNA NEAT1 for diagnosis of high-risk group breast cancer patients**. Curr Probl Cancer 2021:100709.
61. Liang S, Gong X, Zhang G, Huang G, Lu Y, Li Y: **The lncRNA XIST interacts with miR-140/miR-124/iASPP axis to promote pancreatic carcinoma growth**. Oncotarget 2017, **8**:113701–113718.
62. Chen DL, Chen LZ, Lu YX, Zhang DS, Zeng ZL, Pan ZZ, Huang P, Wang FH, Li YH, Ju HQ, Xu RH: **Long noncoding RNA XIST expedites metastasis and modulates epithelial-mesenchymal transition in colorectal cancer**. Cell Death Dis 2017, **8**:e3011.

63. Yao Y, Ma J, Xue Y, Wang P, Li Z, Liu J, Chen L, Xi Z, Teng H, Wang Z, et al: **Knockdown of long non-coding RNA XIST exerts tumor-suppressive functions in human glioblastoma stem cells by up-regulating miR-152**. Cancer Lett 2015, **359**:75–86.
64. Hu C, Liu S, Han M, Wang Y, Xu C: **Knockdown of lncRNA XIST inhibits retinoblastoma progression by modulating the miR-124/STAT3 axis**. Biomed Pharmacother 2018, **107**:547–554.

Figures

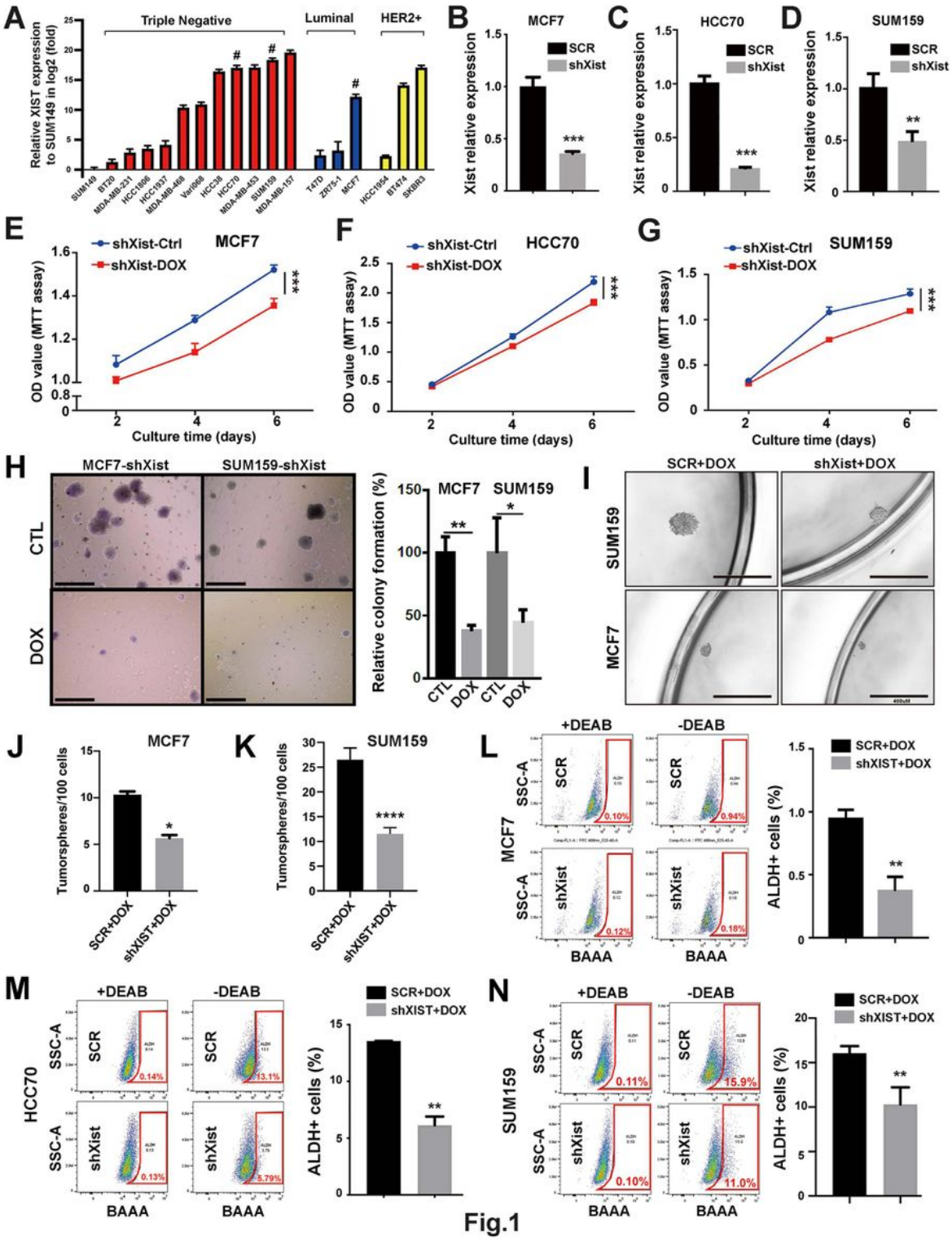

Figure 1

Aberrant *XIST* expression promotes ALDH$^+$ E-CSCs in luminal and TN BC cells. (A) Relative expression of XIST across different subtypes of BC in triple negative (TN), estrogen receptor positive (ER$^+$) luminal, and HER2$^+$ BC cell lines. #: BCCs with relatively high XIST expression selected for DOX-inducible XIST KD. (B-D) DOX-induced XIST KD in MCF7-shXIST (B) HCC70-shXIST (C), and SUM159-shXIST (D) BCCs significantly reduced *XIST* expression compared to DOX-treated cells expressing a SCR sequence. (E-G)

DOX-induced XIST KD in MCF7 (E), HCC70 (F), and SUM159 (G) BCCs modestly reduced cell growth in 2D adherent culture as evaluated by MTT assay. (H) DOX-induced XIST KD markedly reduced colony-forming capacity of MCF7 and SUM159 BCCs embedded in soft agar. Scale bar: 200 μm. (I-K) Tumorsphere formation of MCF7-shXIST (I & J) and SUM159-shXIST (I & K) BCCs vs. corresponding SCR cells grown in ultra-low adherent conditions at clonal density in the presence of 1μg/ml of DOX for 14 days. Tumorspheres with diameter ≥ 40μm were counted. Scale bar: 400 μm. (L-N) DOX-induced KD of XIST in MCF7 (L), HCC70 (M) and SUM159 (N) BCCs significantly reduced the proportion of $ALDH^+$ CSCs. Experiments were repeated three times with similar results and data from one representative experiment are shown. *, **,***: $p<0.05$, 0.01 and 0.001, respectively.

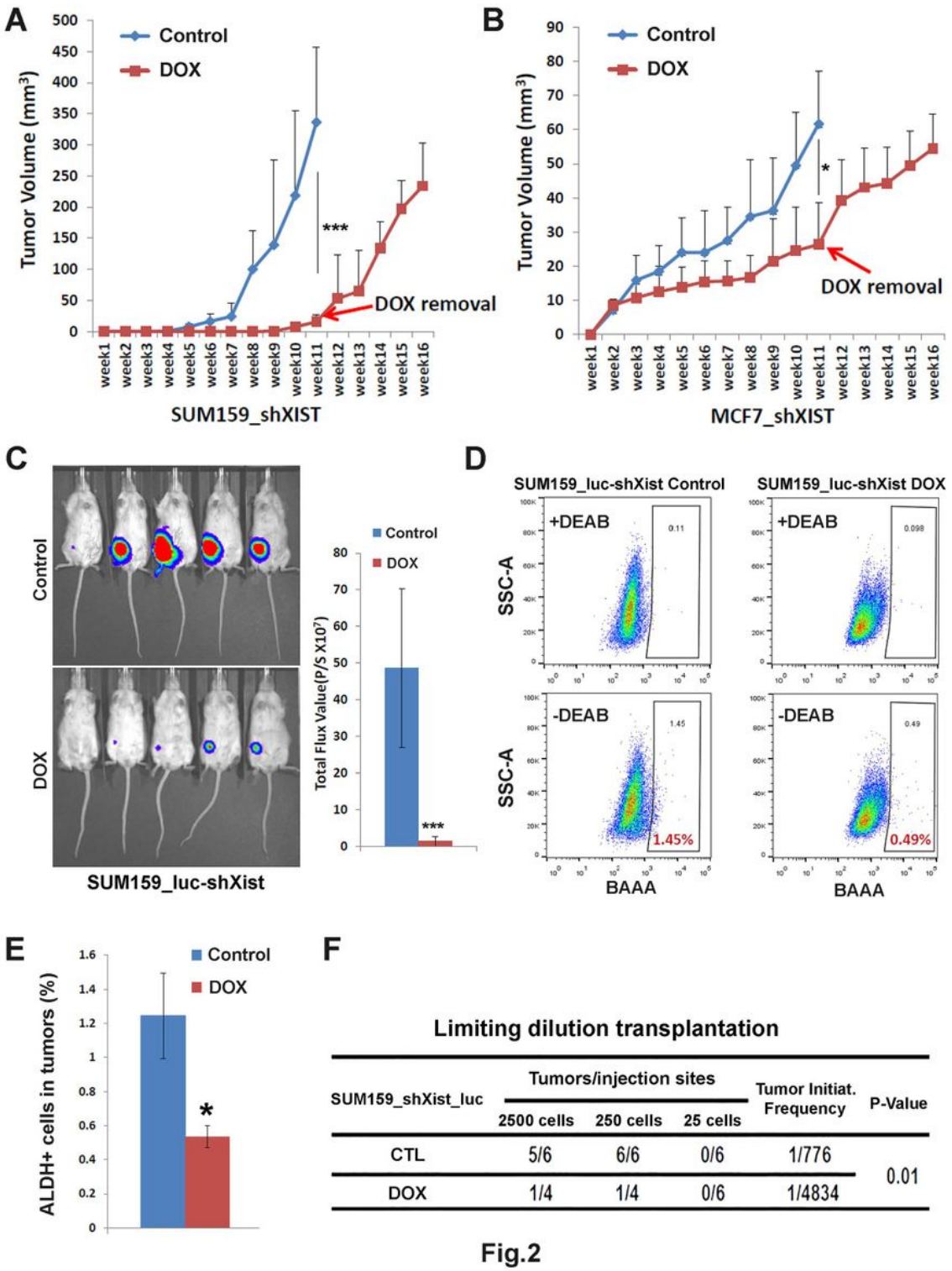

Figure 2

DOX-inducible KD of XIST significantly suppresses tumor growth and tumor-initiating potential in NOD/SCID mice. (A & B) DOX-induced XIST KD significantly abrogated tumor growth of SUM159-shXIST (A) and MCF7-shXIST (B) BCCs in NOD/SCID mice treated with DOX-containing water for 11 weeks, and these mice resumed rapid tumor growth after DOX water removal from week 11-16. (C) Mice implanted with SUM159_Luc-shXIST cells fed with or without DOX containing water for 13 weeks were monitored by

bioluminescence imaging of tumor luciferase activity (C). (D & E) Tumor cells dissociated from tumors of Control and DOX treated mice as shown in Figure C were subjected to ALDEFLOUR assay (D) to determine the percentage of $ALDH^+$ CSCs (E). (F) $H2Kd^+$ mouse stromal cells from pooled tumors of Control or DOX treated mice were gated out by FACS, and live ($DAPI^-$) $H2Kd^-$ SUM159 tumor cells were sorted and subjected to limiting dilution transplantation assay in secondary NOD/SCID mice. *,*** $P < 0.05$ and 0.001 respectively vs. Control.

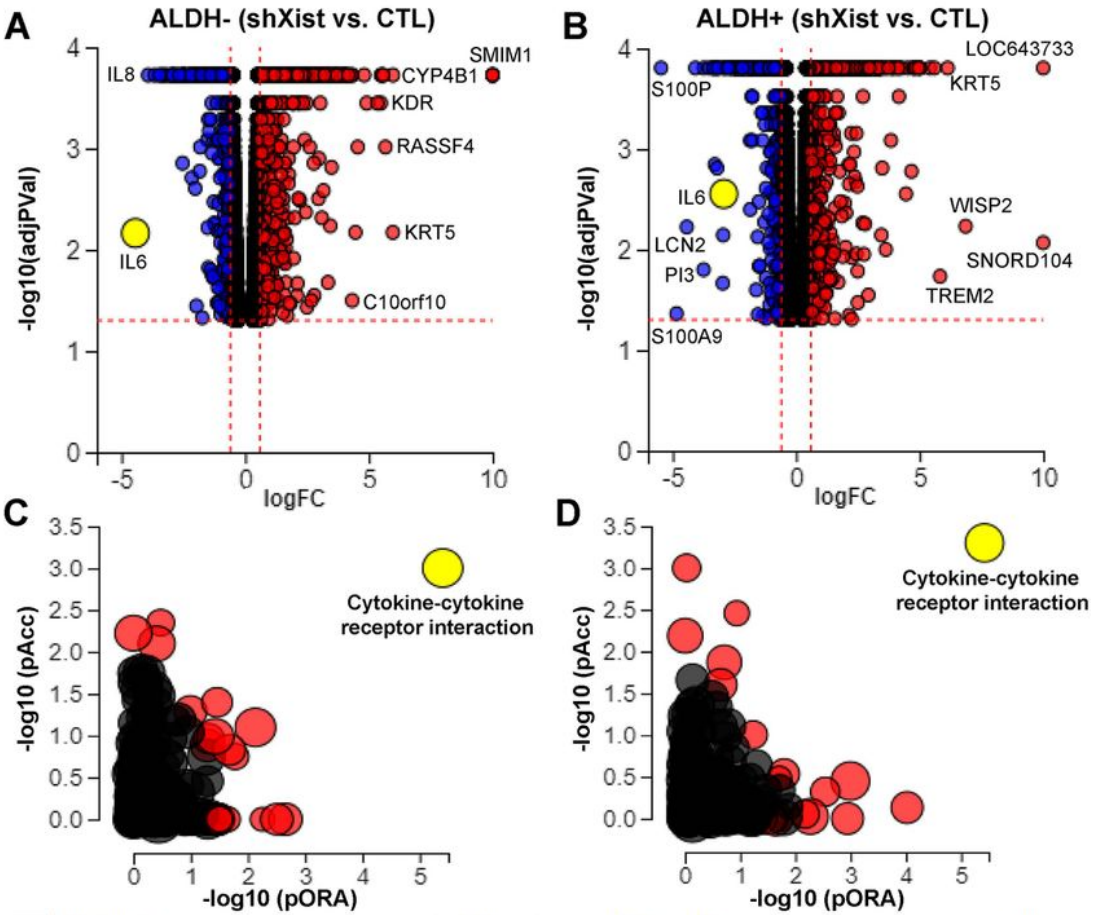

	Pathway Name	p-value
1	Cytokine-cytokine receptor interaction	8.02E-08
2	Chemical carcinogenesis	0.0022057
3	Drug metabolism - cytochrome P450	0.0031154
4	Neuroactive ligand-receptor interaction	0.0049768
5	Selenocompound metabolism	0.0055517
6	Malaria	0.0104698
7	Hippo signaling pathway -multiple species	0.0112727
8	Dorso-ventral axis formation	0.0204005
9	p53 signaling pathway	0.0211894
10	Wnt signaling pathway	0.0211976
11	Protein export	0.0230829
12	Jak-STAT signaling pathway	0.0250613
13	Mismatch repair	0.0313905
14	Ether lipid metabolism	0.0324166
15	Metabolism of xenobiotics by cytochrome P450	0.0324166
16	Leishmaniasis	0.032477
17	NOD-like receptor signaling pathway	0.032918
18	Hematopoietic cell lineage	0.0344472
19	Arachidonic acid metabolism	0.0345233
20	Non-alcoholic fatty liver disease (NAFLD)	0.0366617
21	Rheumatoid arthritis	0.0402853
22	Nicotinate and nicotinamide metabolism	0.0446122

	Pathway Name	p-value
1	Cytokine-cytokine receptor interaction	3.95E-08
2	Rheumatoid arthritis	0.000738721
3	Protein digestion and absorption	0.00113167
4	Neuroactive ligand-receptor interaction	0.00320755
5	Hippo signaling pathway -multiple species	0.00354335
6	Notch signaling pathway	0.00741979
7	NOD-like receptor signaling pathway	0.0104343
8	Wnt signaling pathway	0.0181615
9	beta-Alanine metabolism	0.0196109
10	Cell adhesion molecules (CAMs)	0.0227492
11	Tryptophan metabolism	0.0235603
12	Intestinal immune network for IgA production	0.0250925
13	Hematopoietic cell lineage	0.0295647
14	Leishmaniasis	0.0297407
15	Herpes simplex infection	0.031799
16	Amoebiasis	0.0348633
17	Mineral absorption	0.0355558
18	Malaria	0.0361605
19	Non-alcoholic fatty liver disease (NAFLD)	0.0388511
20	Dorso-ventral axis formation	0.0393704
21	Selenocompound metabolism	0.0411118
22	Chemical carcinogenesis	0.0418947
23	Graft-versus-host disease	0.049575

Fig.3

Figure 3

XIST acts as a master regulator of cytokine-cytokine receptor interaction in $ALDH^-$ and $ALDH^+$ BC cells. (A & B) Significantly downregulated ($log_2FC \leq 0.5$, blue dots) and upregulated ($log_2FC \geq 0.5$, red dots) genes in $ALDH^-$ (A) and $ALDH^+$ (B) cells upon DOX-induced XIST KD, with data presented as volcano plots. (C & D) Significantly changed genes in $ALDH^-$ and $ALDH^+$ BCCs upon DOX-induced XIST KD represent 22 and 23 pathways respectively, and cytokine-cytokine receptor interaction emerged as the most significantly changed pathways in $ALDH^-$ bulk tumor cells (C) and $ALDH^+$ CSCs (D) following DOX-induced XIST KD.

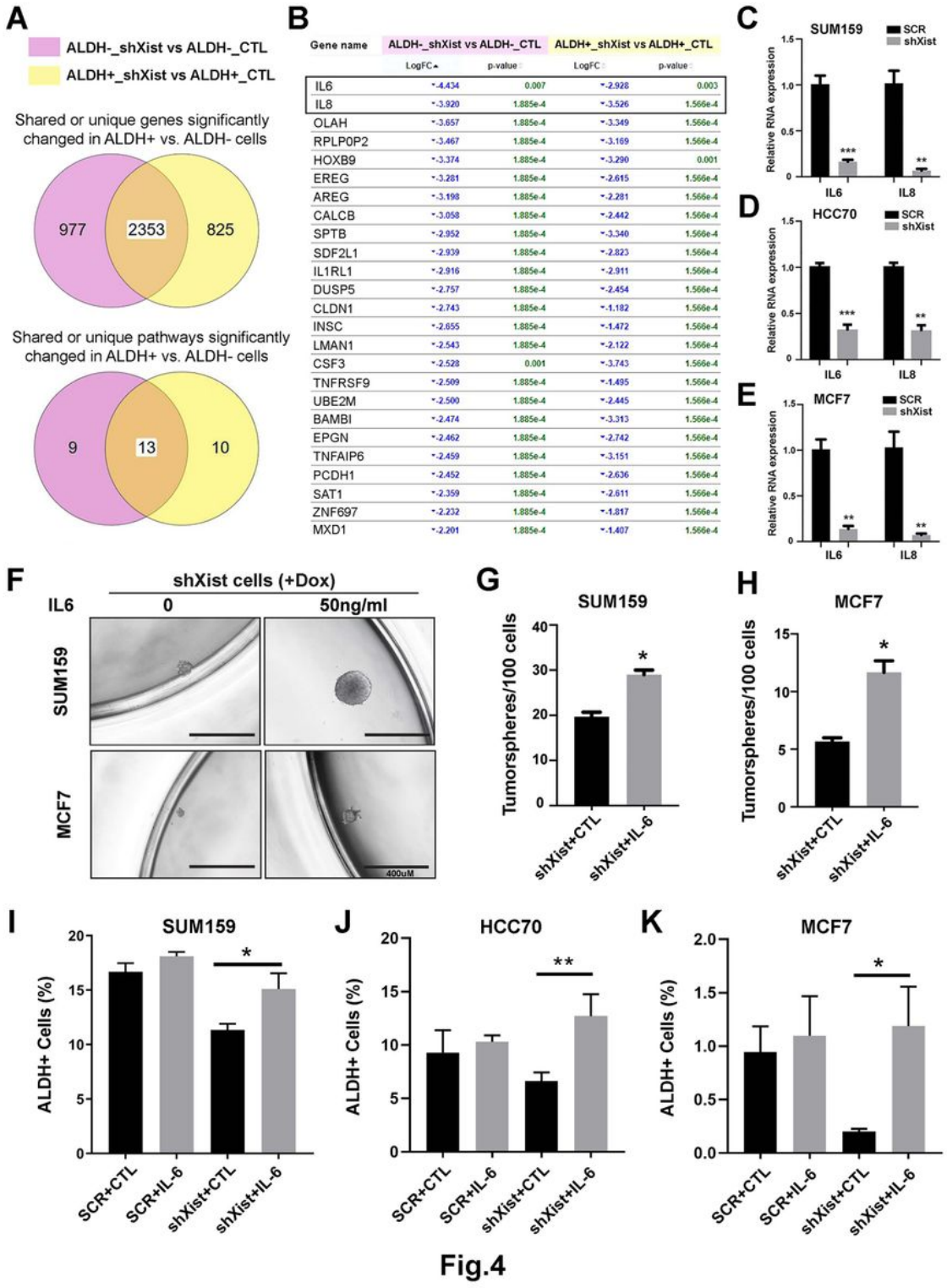

Fig.4

Figure 4

IL-6, but not IL-8, plays a prominent role mediating XIST regulation of ALDH$^+$ E-CSCs. (A) Meta-analysis of the significantly changed genes in SUM159 ALDH$^-$ and ALDH$^+$ cells upon DOX-induced XIST KD revealed 2353 genes shared by ALDH$^-$ and ALDH$^+$ BCCs and 825 genes differentially expressed in ALDH$^+$ CSCs, representing 13 and 10 signaling pathways, respectively. (B) Analysis of the top 25 downregulated genes

shared in $ALDH^-$ vs. $ALDH^+$ cells after DOX-induced XIST KD identified *IL6* and *IL8* as the top 2 genes most significantly downregulated in $ALDH^-$ BCCs and, to a less extent, in $ALDH^+$ CSCs. (C-E) Validation of *IL6* and *IL8* expression in SUM159 (C), HCC70 (D), and MCF7 (E) BCCs following DOX-induced XIST KD by qRT-PCR. (F-H) Exogenous IL-6 rescues the impaired sphere-forming capacity of SUM159 (F & G) and MCF7 BCCs (F & H) subjected to DOX-induced XIST KD. (I) Addition of exogenous IL-6 vs. CTL (water) significantly rescues the decreased percentage of $ALDH^+$ CSCs in DOX-treated SUM159 BCCs expressing shXIST but not SCR sequence. (J & K) Addition of exogenous IL-6 vs. CTL significantly rescues the reduced proportion of $ALDH^+$ CSCs in DOX-treated HCC70 (J) and MCF7 (K) BCCs expressing shXIST but not SCR sequence. Experiments were repeated three times with similar results and qRT-PCR data from one representative experiment are shown. *, **,***: $p<0.05$, 0.01 and 0.001, respectively.

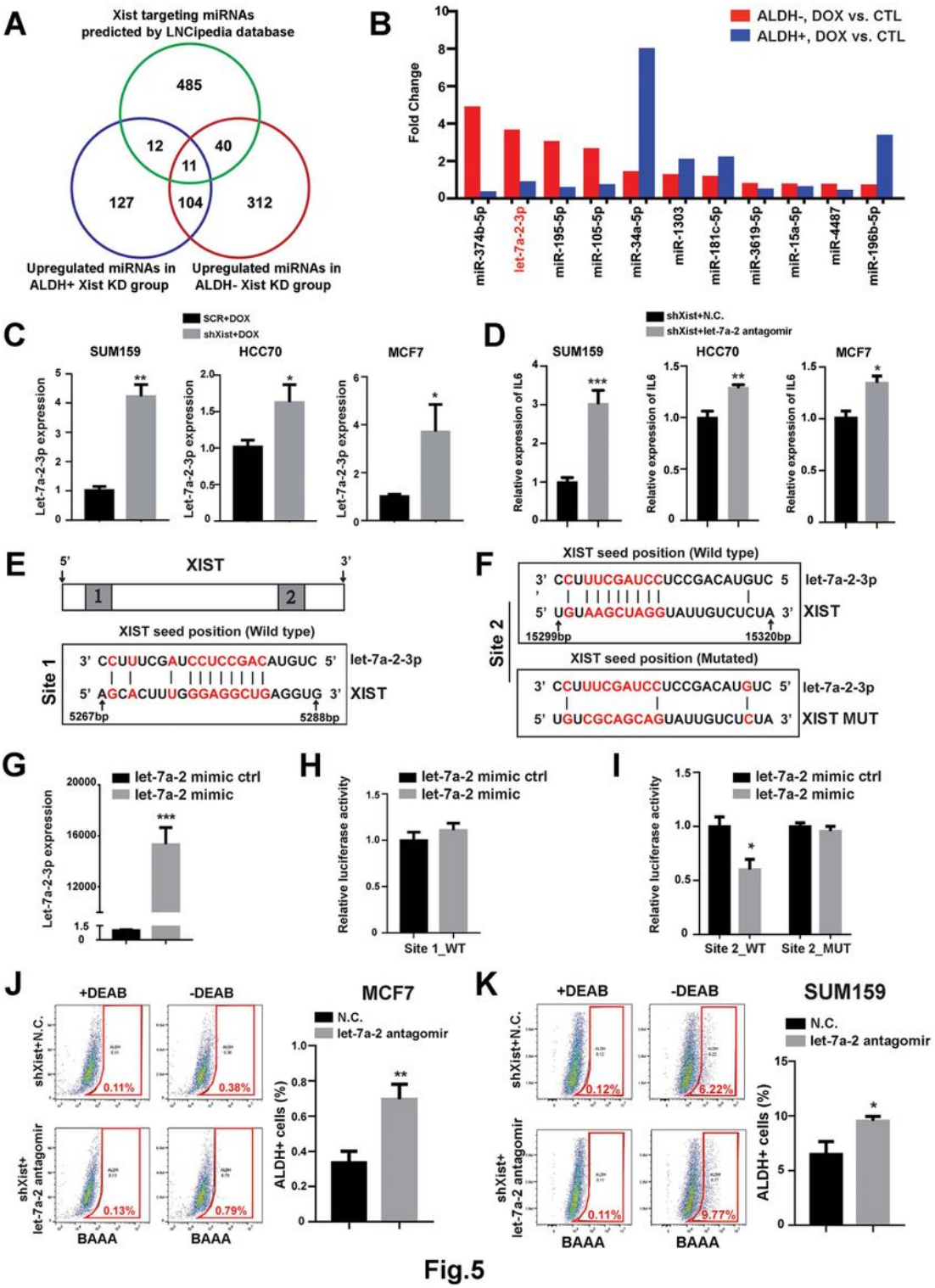

Fig.5

Figure 5

XIST-driven IL-6 expression and increase of ALDH$^+$ CSCs are mediated by its repression of let-7a-2-3p. (A & B) Meta-analysis of the significantly upregulated miRNAs in SUM159 ALDH$^-$ and ALDH$^+$ BCCs upon DOX-induced XIST KD and the potential XIST target miRNAs predicted by the LNCipedia database identified 11 candidate target miRNAs of XIST (A) and fold change of these 11 potential XIST target miRNAs in ALDH$^-$ vs. ALDH$^+$ BCCs upon XIST KD are plotted (B). (C) Validation of let-7a-2-3p expression

in DOX-treated SUM159, HCC70, and MCF70 BCCs expressing shXist vs. a SCR sequence. (D) Transfection of a let-7a-2-3p inhibitor (antagomir) vs. negative control RNA (N.C.) in DOX-treated SUM159-shXIST, HCC70-shXIST and MCF7-shXIST BCCs significantly enhanced *IL-6* expression. (E & F) Sequence alignments of XIST Site 1 (E) and Site 2 (F) with highest probability binding let-7a-2-3p. (G & H) Transfection of a let-7a-2-3p mimic vs. control sequence (ctrl) into SUM159 BCCs markedly increased the expression of let-7a-2-3p (G) and introduction of the let-7a-2-3p mimic failed to inhibit luciferase reporter activity in SUM159 BCCs expressing the luciferase reporter plasmid harboring Site 1 (H). (I) Introduction of the let-7a-2-3p mimic significantly inhibited luciferase reporter activity in SUM159 BCCs transfected with the luciferase reporter plasmid harboring wild-type, but not mutated Site 2. (J & K) DOX-treated MCF7-shXIST (J) and SUM159-shXIST (K) BCCs were transfected with a let-7a-2-3p an inhibitor vs. N.C. and the percentage of $ALDH^+$ CSCs was examined by ALDEFLOUR assay in three independent experiments. *, **,***: $p<0.05$, 0.01 and 0.001, respectively.

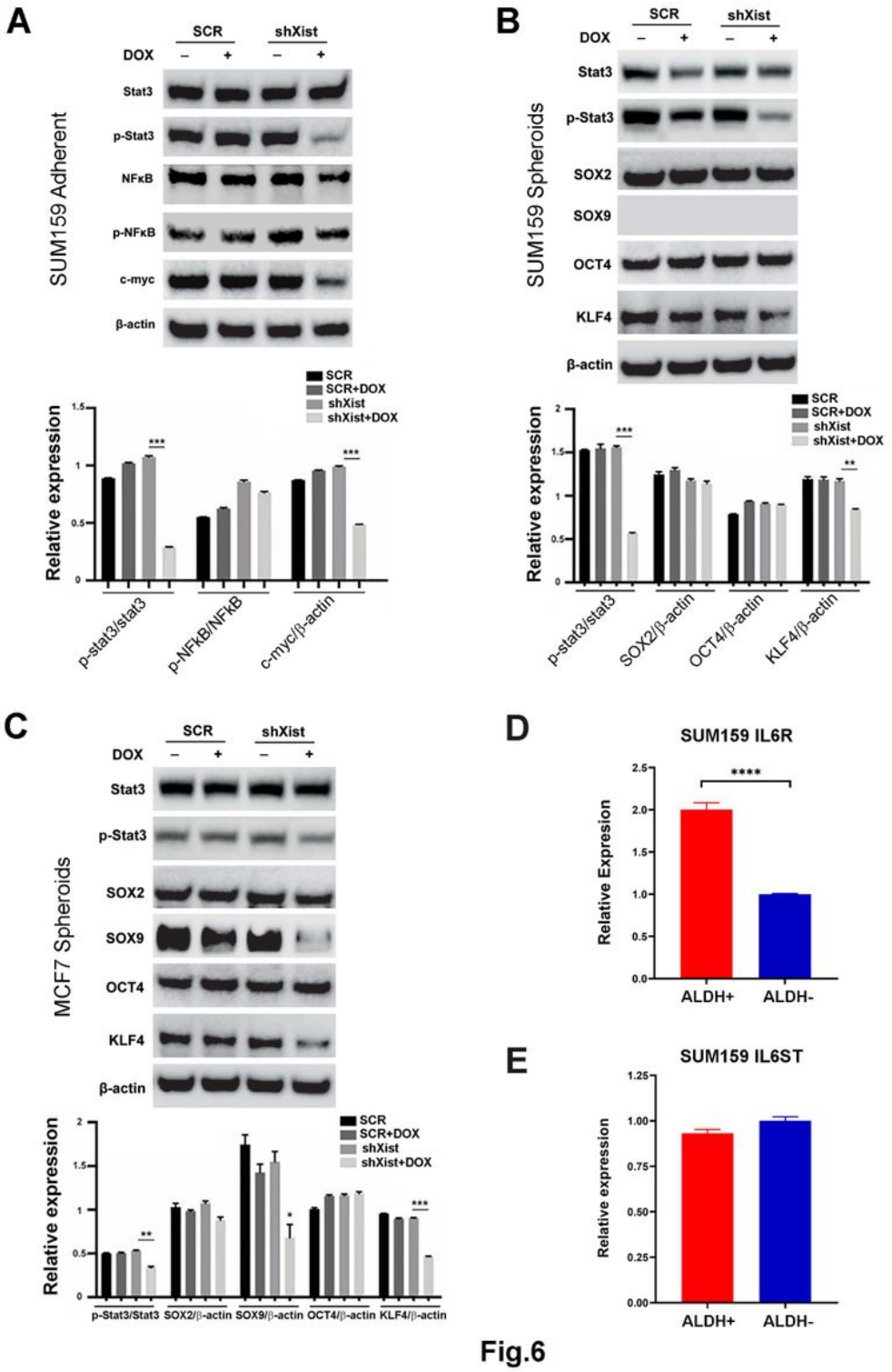

Fig.6

Figure 6

XIST expression in ALDH$^-$ bulk tumor cells drives paracrine IL-6 signaling to promote STAT3 activation and expression of key CSC regulatory factors in ALDH$^+$ CSCs. (A) SUM159 BCCs expressing shXIST vs. a SCR sequence were treated with or without DOX (1μg/ml) for 3 days and subjected to western blotting analysis to examine STAT3 and NFkb activation as well as c-MYC expression. (B & C) Tumorsphere lysates derived from SUM159-shXIST (B) or MCF7-shXIST (C) cells treated with or without DOX (1μg/ml)

for 14 days were examined by immunoblotting with antibodies against STAT3 and pSTAT3 as well as CSC regulatory factors including SOX2, SOX9, OCT4 and KLF4. (D & E) $ALDH^-$ bulk tumor cells and $ALDH^+$ CSCs were FACS sorted and subjected to qRT-PCR analysis to examine the relative expression of *IL6R* (D) and *IL6ST* (E). Statistical significance was determined by a two-tailed unpaired t-test. Experiments were repeated three times independently with similar results, and data from each representative experiment are shown. *, **,***,***: p<0.05, 0.01, 0.001, and 0.0001, respectively.

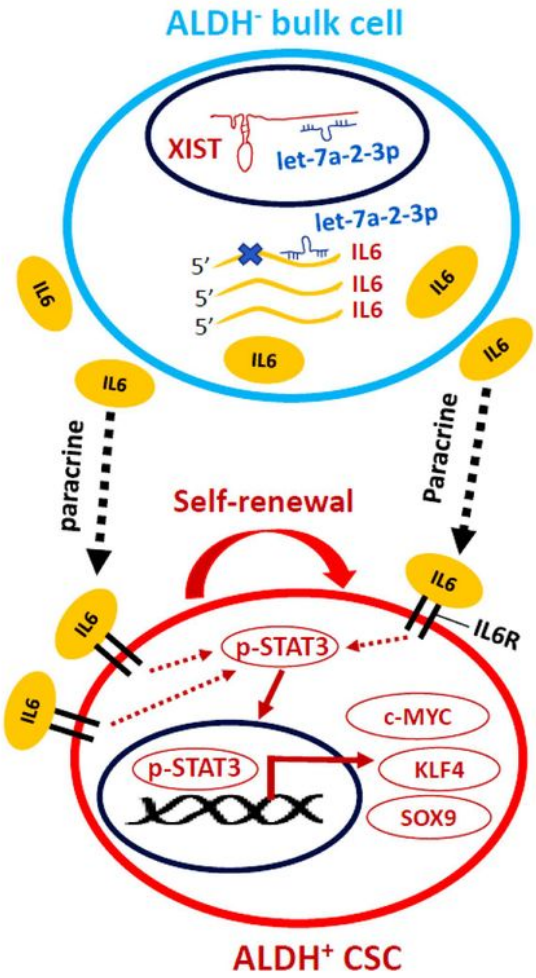

Fig.7

Figure 7

A model illustrating the mechanisms of XIST in regulating ALDH$^+$ E-CSCs. XIST functions as a molecular sponge in the nucleus to sequester let-7a-2-3p, which derepresses let-7a-2-3p mediated inhibition of IL-6 expression in ALDH$^-$ bulk tumor cells. IL-6 produced from ALDH$^-$ bulk tumor cells preferentially binds to IL6R highly expressed on ALDH$^+$ CSCs, which in turn drives STAT3 activation and the expression of key CSC factors including c-MYC, KLF4 and SOX9, promoting self-renewal of ALDH$^+$ CSCs.

Supplementary Files

This is a list of supplementary files associated with this preprint. Click to download.

- SupplementaryFiguresandTables.pdf